

the U.S. Geological Survey Water Availability and Use Science Program

# MODFLOW 6 – Supplemental Technical Information

Version mf6.4.4—February 13, 2024

U.S. Department of the Interior  
U.S. Geological Survey

**Cover.** Binary computer code illustration.

# Contents

<b>Chapter 1. Introduction</b>	1-1
<b>Chapter 2. Specific Discharge</b>	2-1
Estimating the $z$ Component of Velocity (Specific Discharge)	2-1
Estimating the $x$ and $y$ Components of Velocity (Specific Discharge)	2-1
Weights	2-3
<b>Chapter 3. Drain Package Discharge Scaling</b>	3-1
Theory	3-1
Example Drain Discharge Scaling Calculations	3-4
Incorporation of the modified Drain (DRN) Package into the CVFD Groundwater Flow Equation	3-4
Standard Formulation	3-5
Newton-Raphson Formulation	3-6
Use of Drain Discharge Scaling	3-6
The original drain package formulation with a specified drainage depth value	3-6
Groundwater seepage from the Unsaturated Zone Flow Package	3-6
<b>Chapter 4. Multi-Aquifer Well Package Connection Flow Correction</b>	4-1
Multi-Aquifer Well Flow Correction	4-1
Incorporation of the Flow Correction into the CVFD Groundwater Flow Equation	4-1
Standard Formulation	4-1
Newton-Raphson Formulation	4-3
Newton-Raphson formulation when $HMAW_i$ is the Downstream Head	4-4
Newton-Raphson formulation when $h_n$ is the Downstream Head	4-5
<b>Chapter 5. Storage Package Modifications</b>	5-1
Original Approach	5-1
Revised Formulation	5-3
Incorporation of the Revised Specific Storage Formulation into the CVFD Groundwater Flow Equation	5-4
Standard Formulation	5-5
Newton-Raphson Formulation	5-5
<b>Chapter 6. Time-Varying Hydraulic Conductivity and Storage</b>	6-1
Storage Change Integration: Specific Storage	6-1
Standard Formulation	6-2
Newton-Raphson Formulation	6-2
Storage Change Integration: Specific Yield	6-3
Standard Formulation	6-3
Newton-Raphson Formulation	6-3
<b>Chapter 7. Generalized Coupling of Numerical Models</b>	7-1
The Interface Model	7-1

<b>Chapter 8. Accounting for Fluid Viscosity .....</b>	<b>8–1</b>
Dependence of Viscosity on Concentration and Temperature .....	8–2
Accounting for Variable Viscosity in Flows Between Cells .....	8–3
Accounting for Variable Viscosity in Boundary Flows .....	8–3
<b>Chapter 9. Revised Parameterization of Transport for Combined Mobile and Immobile Domain Simulations .....</b>	<b>9–1</b>
Review of the Original Parameterization .....	9–1
Revised Parameterization .....	9–3
Revised Parameters .....	9–5
Conversion of Existing Model Input to the Revised Parameterization .....	9–6
Simulation Without Immobile Domains .....	9–6
Simulation With At Least One Immobile Domain .....	9–7
Unrealistic Parameter Values .....	9–7
References Cited .....	R–1

## Figures

3–1. Graphs showing combined linear and cubic scaling functions for drain discharge and the derivatives of the linear and cubic scaling fraction functions .....	3–2
3–2. Graphs showing a conceptual model cell using scaled drain discharge and the relation between the groundwater level and drain discharge .....	3–5
4–1. Graph showing the downstream head transition functions used to correct the multi-aquifer flow for a connection .....	4–2
5–1. Graph showing changes in the flow from specific storage that result from changing the vertical datum .....	5–2
7–1. A plan view of the model grid from MT3DMS problem 10 .....	7–2
7–2. A top view of the Interface Model grid .....	7–3
7–3. Stencil size and the extent of the Interface Model grid .....	7–4
8–1. Graph showing the nonlinear response in the viscosity as temperature changes .....	8–3

## Tables

1–1. MODFLOW 6 enhancements .....	1–1
9–1. Symbols, descriptions, and definitions of original mobile and immobile domain model parameters (used in versions of MODFLOW 6 up to and including version 6.4.1) that are affected by the revised parameterization. In the original parameterization, division of the aquifer into domains is conceptualized in terms of solid mass fractions, and domain properties are defined on a per-aquifer-volume basis .....	9–3

- 9–2. Symbols, descriptions, and definitions of revised mobile and immobile domain model parameters introduced in MODFLOW 6 version 6.4.2. In the revised parameterization, division of the aquifer into domains is conceptualized in terms of volume fractions, and domain properties are defined on a per-domain-volume basis ..... 9–5

Blank page

# Chapter 1. Introduction

This document is a technical reference document that describes the motivation and implementation of functionality added to MODFLOW 6 since the initial release ([Hughes and others, 2017](#); [Langevin and others, 2017](#)) and not documented in separate U.S. Geological Survey publications, for example [Provost and others \(2017\)](#). Examples have been included for the MODFLOW 6 components summarized in table 1–1.

**Table 1–1.** MODFLOW 6 enhancements.

MODFLOW 6 enhancements	Chapter	Initial MODFLOW 6 version	Latest update – MODFLOW 6 version
Specific Discharge	<a href="#">2</a>	6.0.2	6.1.0
DRN Package	<a href="#">3</a>	6.1.1	–
Discharge Scaling			
MAW Package			
Connection Flow Correction	<a href="#">4</a>	6.1.1	–
STO Package Specific Storage Revision	<a href="#">5</a>	6.1.3	–
TVK and TVS Capabilities for NPF	<a href="#">6</a>	6.3.0	–
Generalized Coupling of Numerical Models	<a href="#">7</a>	6.3.0	–
VSC Package Revised Parameterization of Transport for Combined Mobile and Immobile Domain Simulations	<a href="#">8</a> <a href="#">9</a>	6.4.0 6.4.2	–

## Chapter 2. Specific Discharge

A MODFLOW 6 flow simulation calculates the flow of water across all interfaces between cells. The flow reported for a given cell-cell interface is the component of the flow vector normal to the interface. The normal component of the specific discharge ( $L/T$ ), or Darcy velocity, which we shorten here to "velocity," is obtained by dividing the normal component of flow by the interface area. The velocity vector at the center of a cell can then be estimated by interpolating component information from all the interfaces of the cell.

The velocity interpolation scheme presented here is an adaptation and simplification of the gradient interpolation scheme used in the XT3D capability of MODFLOW 6 ([Provost and others, 2017](#)). In XT3D, the three-dimensional head-gradient vector is estimated at a point on the interface between two cells using gradient-component information from the connections between each of those two cells and its neighboring cells. In this velocity interpolation scheme, the three-dimensional velocity vector is estimated at the center of a cell using velocity-component information from the cell-cell interfaces of the cell. (The scheme does not currently include velocity-component information from "external" faces of a cell but could be modified to do so.) The assembly of component information and the weighting scheme in the velocity interpolation are similar to those in the XT3D gradient interpolation: the greatest weight is given to component information from points that are closest to the cell center and whose directions are most closely aligned with the desired velocity component. In XT3D, gradient components are initially estimated in a coordinate system aligned with the connection between two cells, whereas in the velocity interpolation the components are estimated directly in  $(x, y, z)$  model coordinates. This simplifies the notation somewhat and, more importantly, allows the  $z$  component to be treated separately from the  $x$  and  $y$  components using information only from the horizontal interfaces of the cell (those along the top or bottom of the cell), which are the only interfaces that provide  $z$ -component information.

### Estimating the $z$ Component of Velocity (Specific Discharge)

The  $z$  component of velocity ( $L/T$ ) at the cell center,  $v^z$ , is estimated by calculating a weighted average of the  $z$  components of velocity at the horizontal interfaces of the cell:

$$v^z = \sum_{k=1}^{N_H} \phi_k^z v_k^z, \quad (2-1)$$

where the summation is over the horizontal interfaces of the cell, which are locally indexed by  $k = 1, \dots, N_H$ ,  $v_k^z$  is the  $z$  component of velocity ( $L/T$ ) at horizontal interface  $k$ , and  $\phi_k^z$  is the weight (unitless) assigned to  $v_k^z$ . (Weights are discussed in detail in the "[Weights](#)" section below.)

### Estimating the $x$ and $y$ Components of Velocity (Specific Discharge)

The development in this section closely parallels the development in equations 9 through 16 in [Provost and others \(2017\)](#). The present development has been adapted specifically for interpolation of the velocity vector at a cell center in  $(x, y, z)$  model coordinates and is simplified by the separate treatment of the  $z$  component described in the previous section.

The vertical interfaces of a cell (those along the "sides" of the cell), which are locally indexed by  $i = 1, \dots, N_V$ , provide normal-component information that is used to estimate the  $x$  and  $y$  components of the velocity at the cell center. By definition,  $v_i^n$ , the normal component of velocity ( $L/T$ ) at vertical interface  $i$ , is related to the three-dimensional velocity vector by

## 2–2 MODFLOW 6 – Supplemental Technical Information

$$\mathbf{n}_i^T \mathbf{v}_i = v_i^n, \quad (2-2)$$

where superscript “T” indicates the transpose, and the left-hand side of equation 2–2 is the scalar product (or “dot product”) of  $\mathbf{n}_i$ , the unit vector (unitless) normal to interface  $i$ , and  $\mathbf{v}_i$ , the velocity vector ( $L/T$ ) at interface  $i$ . Expanding equation 2–2 in terms of vector components gives

$$n_i^x v_i^x + n_i^y v_i^y + n_i^z v_i^z = v_i^n. \quad (2-3)$$

where  $n_i^x$ ,  $n_i^y$ , and  $n_i^z$  are, respectively, the  $x$ ,  $y$ , and  $z$  components of  $\mathbf{n}_i$ , and  $v_i^x$ ,  $v_i^y$ , and  $v_i^z$  are, respectively, the  $x$ ,  $y$ , and  $z$  components of  $\mathbf{v}_i$ . Recognizing that  $n_i^z = 0$  for a vertical interface and solving equation 2–3 for the  $x$  component of velocity gives

$$v_i^x = (v_i^n - n_i^y v_i^y) / n_i^x. \quad (2-4)$$

The expression for  $v_i^x$  in equation 2–4 is based on information solely from vertical interface  $i$ . However, the  $y$  component,  $v_i^y$ , which appears on the right-hand side of equation 2–4, is unknown and cannot be deduced based on information from interface  $i$  alone. Therefore, it is assumed that the  $y$  component of velocity ( $L/T$ ) at the cell center,  $v^y$ , which is also unknown at this point but will eventually be estimated, may be substituted into equation 2–4 as an approximation to  $v_i^y$ . The  $x$  component of velocity ( $L/T$ ) at the cell center,  $v^x$ , is then estimated by calculating a weighted average of the  $x$  components of velocity at all the vertical interfaces:

$$v^x = \sum_{i=1}^{N_V} \phi_i^x v_i^x = \sum_{i=1}^{N_V} \frac{\phi_i^x v_i^n}{n_i^x} - \left( \sum_{i=1}^{N_V} \frac{\phi_i^x n_i^y}{n_i^x} \right) v^y, \quad (2-5)$$

where  $\phi_i^x$  is the weight (unitless) assigned to  $v_i^x$ . Analogous consideration of the  $y$  component of velocity ( $L/T$ ) at the cell center,  $v^y$ , produces the weighted average

$$v^y = \sum_{i=1}^{N_V} \phi_i^y v_i^y = \sum_{i=1}^{N_V} \frac{\phi_i^y v_i^n}{n_i^y} - \left( \sum_{i=1}^{N_V} \frac{\phi_i^y n_i^x}{n_i^y} \right) v^x, \quad (2-6)$$

where  $\phi_i^y$  is the weight (unitless) assigned to  $v_i^y$ . (Weights are discussed in detail in the “Weights” section below.) There are now two equations, 2–5 and 2–6, that can be solved for the two unknowns,  $v^x$  and  $v^y$ , to give

$$v^x = \frac{1}{1 - A^{xy} A^{yx}} \sum_{i=1}^{N_V} (B_i^x - A^{xy} B_i^y) v_i^n \quad (2-7)$$

$$v^y = \frac{1}{1 - A^{xy} A^{yx}} \sum_{i=1}^{N_V} (B_i^y - A^{yx} B_i^x) v_i^n, \quad (2-8)$$

where

$$A^{xy} = \sum_{i=1}^{N_V} B_i^x n_i^y \quad (2-9)$$

$$A^{yx} = \sum_{i=1}^{N_V} B_i^y n_i^x, \quad (2-10)$$

and

$$B_i^x = \frac{\phi_i^x}{n_i^x} \quad (2-11)$$

$$B_i^y = \frac{\phi_i^y}{n_i^y}. \quad (2-12)$$

Equations 2-7 and 2-8, with the coefficients given by equations 2-9 through 2-12, are the expressions used to estimate the  $x$  and  $y$  components of the velocity vector at the cell center based on normal-component information at the vertical interfaces of the cell.

## Weights

For estimation of the  $z$  component of velocity as a weighted average, we define a set of weights (unitless) based on the shortest distance ( $L$ ),  $D_k$ , from the cell center to each horizontal interface  $k$  as follows:

$$\omega_k^z = 1 - \frac{D_k}{\sum_{m=1}^{N_H} D_m}. \quad (2-13)$$

Interfaces that are closest to the cell center receive the greatest weights. Before incorporating the weights into equation 2-1, we normalize them so they sum to 1:

$$\phi_k^z = \frac{\omega_k^z}{N_H - 1} = \frac{1}{N_H - 1} \left( 1 - \frac{D_k}{\sum_{m=1}^{N_H} D_m} \right). \quad (2-14)$$

For estimation of the  $x$  and  $y$  components of velocity, we define a set of weights (unitless) that take into account not only distance from the cell center, but also how closely the normal-component information at each vertical interface aligns with the velocity component ( $x$  or  $y$ ) being expressed as a weighted average. For the  $x$  component of velocity the weights are

$$\omega_i^x = \left[ 1 - \frac{D_i |n_i^x|}{\sum_{l=1}^{N_V} D_l |n_l^x|} \right] |n_i^x| = \left[ \frac{\sum_{l=1}^{N_V} D_l |n_l^x| - D_i |n_i^x|}{\sum_{l=1}^{N_V} D_l |n_l^x|} \right] |n_i^x|, \quad (2-15)$$

and for the  $y$  component of velocity the weights are

## 2-4 MODFLOW 6 – Supplemental Technical Information

$$\omega_i^y = \left[ 1 - \frac{D_i |n_i^y|}{\sum_{l=1}^{N_V} D_l |n_l^y|} \right] |n_i^y| = \left[ \frac{\sum_{l=1}^{N_V} D_l |n_l^y| - D_i |n_i^y|}{\sum_{l=1}^{N_V} D_l |n_l^y|} \right] |n_i^y|. \quad (2-16)$$

Interfaces that are closest to the cell center and align most closely with the component direction ( $x$  or  $y$ ) for which they are being used receive the greatest weights. The corresponding normalized weights used in equations 2-11 and 2-12 are:

$$\phi_i^x = \frac{\omega_i^x |n_i^x|}{\sum_{l=1}^{N_V} \omega_l^x |n_l^x|} \quad (2-17)$$

and

$$\phi_i^y = \frac{\omega_i^y |n_i^y|}{\sum_{l=1}^{N_V} \omega_l^y |n_l^y|}, \quad (2-18)$$

respectively. Substitution of equations 2-15 and 2-16 into equations 2-17 and 2-18, followed by substitution of equations 2-17 and 2-18 into equations 2-11 and 2-12, and simplification results in the following expressions for the coefficients  $B_i^x$  and  $B_i^y$ :

$$B_i^x = \frac{\left[ \sum_{l=1}^{N_V} D_l |n_l^x| - D_i |n_i^x| \right] |n_i^x| \operatorname{sign}(n_i^x)}{\sum_{j=1}^{N_V} \left[ \sum_{l=1}^{N_V} D_l |n_l^x| - D_j |n_j^x| \right] |n_j^x| |n_j^x|} \quad (2-19)$$

and

$$B_i^y = \frac{\left[ \sum_{l=1}^{N_V} D_l |n_l^y| - D_i |n_i^y| \right] |n_i^y| \operatorname{sign}(n_i^y)}{\sum_{j=1}^{N_V} \left[ \sum_{l=1}^{N_V} D_l |n_l^y| - D_j |n_j^y| \right] |n_j^y| |n_j^y|}, \quad (2-20)$$

where  $\operatorname{sign}(n)$  equals +1, 0, or -1 when  $n$  is positive, zero, or negative, respectively.

## Chapter 3. Drain Package Discharge Scaling

In the original release of the MODFLOW 6 Drain (DRN) Package a drain is designed to simulate the effects of agricultural drains, springs, and other features that remove water from the aquifer at a rate proportional to the difference between the head in the aquifer and some fixed head or elevation, called the drain elevation, so long as the head in the aquifer is above that elevation. If, however, the aquifer head falls below the drain elevation, then the drain has no effect on the aquifer. The constant of proportionality is called the drain conductance. This chapter describes a new feature of the MODFLOW 6 DRN Package that allows the drain conductance to gradually increase from zero to the user-specified value as a function of the simulated groundwater head.

### Theory

The standard drain equation in MODFLOW 6 is

$$Q_{out,nb} = \begin{cases} 0 & h_n \leq HDRN_{nb} \\ CDRN_{nb} (h_n - HDRN_{nb}) & h_n > HDRN_{nb} \end{cases}, \quad (3-1)$$

where  $Q_{out,nb}$  is the flow from the aquifer to drain  $nb$  ( $L^3 T^{-1}$ ),  $CDRN_{nb}$  is the drain conductance ( $L^2 T^{-1}$ ),  $HDRN_{nb}$  is the drain elevation ( $L$ ), and  $h_n$  is the head in the cell containing the drain ( $L$ ). Equation 3-1 rewritten in terms of flow from the drain into aquifer ( $L^3 T^{-1}$ ),  $QDRN$ , is

$$QDRN_{nb} = \begin{cases} CDRN_{nb} (HDRN_{nb} - h_n) & h_n > HDRN_{nb} \\ 0 & h_n \leq HDRN_{nb} \end{cases}. \quad (3-2)$$

The standard DRN Package has been modified to include the option to scale the drain conductance using either linear or cubic scaling. The modified form of the drain equation (eq. 3-2) with linear scaling is

$$QDRN_{nb} = F_{DRN_{nb}} CDRN_{nb} (ZDRN_{nb} - h_n), \quad (3-3)$$

where  $ZDRN_{nb}$  is the elevation at which drainage discharge begins ( $L$ ), and  $F_{DRN_{nb}}$  is the linear scaling function (unitless), which accounts for how the conductance of the drain changes with changes in head. Conceptually, the drain conductance changes because the area through which flow occurs depends on the head. The area through which flow occurs increases as the head at the drain increases. The linear scaling function is defined as

$$F_{DRN_{nb}} = \begin{cases} 0 & \Delta h_{n,nb}^r \leq 0 \\ \Delta h_{n,nb}^r & 0 < \Delta h_{n,nb}^r < 1, \\ 1 & \Delta h_{n,nb}^r \geq 1 \end{cases}, \quad (3-4)$$

where  $DDRN_{nb}$  is the drainage depth ( $L$ ) and the relative drain head difference ( $L$ ) is defined as

$$\Delta h_{n,nb}^r \equiv \frac{h_n - ZDRN_{nb}}{|DDRN_{nb}|}. \quad (3-5)$$

### 3–2 MODFLOW 6 – Supplemental Technical Information

The elevation at which drainage begins,  $ZDRN_{nb}$  depends on whether the drainage depth,  $DDRN_{nb}$ , is positive or negative and is calculated as

$$ZDRN_{nb} = \begin{cases} HDRN_{nb} - |DDRN_{nb}| & DDRN_{nb} < 0, \\ HDRN_{nb} & DDRN_{nb} \geq 0 \end{cases} \quad (3-6)$$

If  $DDRN_{nb}$  is positive,  $ZDRN_{nb}$  is the drain elevation just as it is in the standard formulation. If  $DDRN_{nb}$  is negative,  $ZDRN_{nb}$  is the drain elevation plus the (negative) drainage depth. If  $DDRN_{nb}$  is zero, the standard formulation is used. The linear scaling function ( $F_{DRN_{nb}}$ ) is shown in figure 3–1.

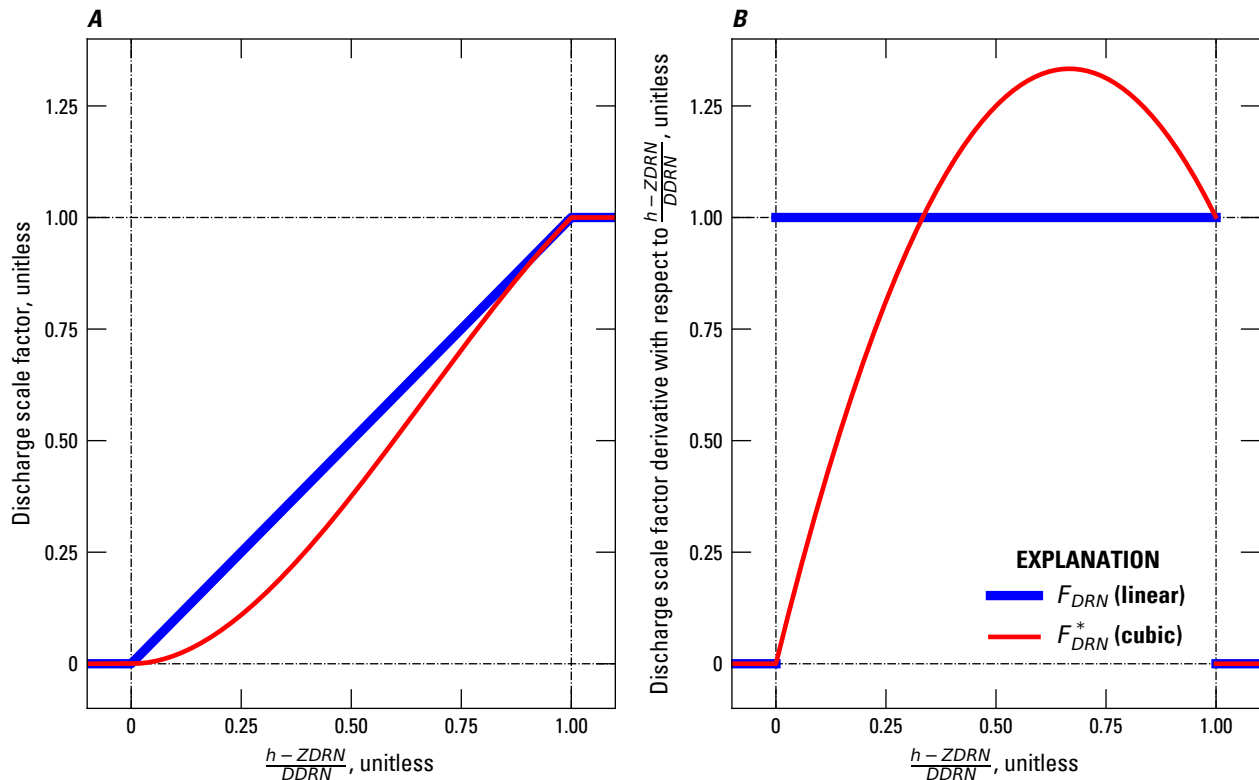


**Figure 3–1.** Graphs showing combined linear and cubic scaling functions for drain discharge and the derivatives of the linear and cubic scaling fraction functions. *A*, linear and cubic fraction functions and *B*, derivatives of the linear and cubic scaling functions with respect to the relative drain head difference ( $\frac{h - ZDRN}{|DDRN|}$ ). The derivative of the linear and cubic scaling functions with respect to  $h$  is the product of the derivative with respect to  $\frac{h - ZDRN}{|DDRN|}$  and  $\frac{1}{|DDRN|}$ .

The linear scaling function varies with head according to equations 3–4 and 3–5. Differentiation of equation 3–4 with respect to  $h_n$ , with application of the chain rule to account for the variation of  $\Delta h_{n,nb}^r$  with respect to  $h_n$  in equation 3–5, gives

$$\frac{\partial F_{DRN_{nb}}}{\partial h_n} = \begin{cases} 0 & \Delta h_{n,nb}^r \leq 0 \\ \frac{1}{|DDRN_{nb}|} & 0 < \Delta h_{n,nb}^r < 1, \\ 1 & \Delta h_{n,nb}^r \geq 1 \end{cases} \quad (3-7)$$

which is discontinuous in the neighborhood of  $h_n = ZDRN_{nb}$  and  $h_n = ZDRN_{nb} - |DDRN_{nb}|$ . The derivative of the linear scaled drain discharge (eq. 3-3) with respect to  $h_n$  is

$$\frac{\partial QDRN_{nb}}{\partial h_n} = -F_{DRN_{nb}} CDRN_{nb} + \frac{\partial F_{DRN_{nb}}}{\partial h_n} CDRN_{nb} (ZDRN_{nb} - h_n). \quad (3-8)$$

Substitution of equations 3-4 and 3-7 into equation 3-8 results in

$$\frac{\partial QDRN_{nb}}{\partial h_n} = \begin{cases} 0 & \Delta h_{n,nb}^r \leq 0 \\ -2 CDRN_{nb} \Delta h_{n,nb}^r & 0 < \Delta h_{n,nb}^r < 1, \\ -CDRN_{nb} & \Delta h_{n,nb}^r \geq 1 \end{cases} \quad (3-9)$$

which remains discontinuous in the vicinity of  $ZDRN_{nb}$ .

When the Newton-Raphson formulation is used, discontinuous derivatives can cause non-convergence in the neighborhood of the discontinuity (Kavetski and Kuczera, 2007). To ensure continuous drain discharge derivatives when the Newton-Raphson formulation is used, cubic smoothing of the linear relative drain head difference is used and equation 3-3 is modified to

$$QDRN_{nb}^* = F_{DRN_{nb}}^* CDRN_{nb} (ZDRN_{nb} - h_n), \quad (3-10)$$

where where  $F_{DRN_{nb}}^*$  is the cubic scaling function. The cubic scaling function is defined as

$$F_{DRN_{nb}}^* = \begin{cases} 0 & \Delta h_{n,nb}^r \leq 0 \\ -(\Delta h_{n,nb}^r)^3 + 2(\Delta h_{n,nb}^r)^2 & 0 < \Delta h_{n,nb}^r < 1, \\ 1 & \Delta h_{n,nb}^r \geq 1 \end{cases} \quad (3-11)$$

which is continuous in the vicinity of  $h_n = ZDRN_{nb}$  and  $h_n = ZDRN_{nb} - |DDRN_{nb}|$  (fig. 3-1A). The derivative of equation 3-11 with respect to  $h_n$  is

$$\frac{\partial F_{DRN_{nb}}^*}{\partial h_n} = \begin{cases} 0 & \Delta h_{n,nb}^r \leq 0 \\ -\frac{3}{|DDRN_{nb}|} (\Delta h_{n,nb}^r)^2 + & \\ \frac{4}{|DDRN_{nb}|} \Delta h_{n,nb}^r & 0 < \Delta h_{n,nb}^r < 1, \\ 0 & \Delta h_{n,nb}^r \geq 1 \end{cases}, \quad (3-12)$$

### 3–4 MODFLOW 6 – Supplemental Technical Information

which is discontinuous in the vicinity of  $h_n = ZDRN_{nb} - |DDRN_{nb}|$  (fig. 3–1B). The derivative of the cubic scaled drain discharge (eq. 3–10) with respect to  $h$  is

$$\frac{\partial QDRN_{nb}^*}{\partial h} = -F_{DRN_{nb}}^* CDRN_{nb} + \frac{\partial F_{DRN_{nb}}^*}{\partial h} CDRN_{nb} (ZDRN_{nb} - h_n). \quad (3-13)$$

Substitution of equations 3–11 and 3–12 into equation 3–13 results in

$$\frac{\partial QDRN_{nb}^*}{\partial h_n} = \begin{cases} 0 & \Delta h_{n,nb}^r \leq 0 \\ -CDRN_{nb} \left[ -(\Delta h_{n,nb}^r)^3 + 2(\Delta h_{n,nb}^r)^2 \right] + \\ CDRN_{nb} \left[ -\frac{3}{DDRN_{nb}} (\Delta h_{n,nb}^r)^2 + \right. \\ \left. \frac{4}{DDRN_{nb}} (\Delta h_{n,nb}^r) \right] (ZDRN_{nb} - h_n) & 0 < \Delta h_{n,nb}^r < 1 \\ -CDRN_{nb} & \Delta h_{n,nb}^r \geq 1 \end{cases}, \quad (3-14)$$

which is continuous in the vicinity of  $h_n = ZDRN_{nb}$  and  $h_n = ZDRN_{nb} - |DDRN_{nb}|$ .

### Example Drain Discharge Scaling Calculations

An example of the differences between the standard, linearly-scaled, and cubically-scaled drainage discharge are shown in figure 3–2. In this example the elevation that drainage discharge starts ( $ZDRN$ ) is set at  $\frac{DDRN}{2}$  below land surface elevation and drainage discharge is equal for all approaches at  $ZDRN + DDRN$  (fig. 3–2A). In this conceptual problem, the groundwater head linearly increases from a value less than  $ZDRN$  to greater than  $ZDRN + DDRN$  during the simulation, which is presented as the head difference ( $h - ZDRN$ ) divided by the drainage depth in figure 3–2B. The drainage discharge that results from the linear increase in groundwater head using the original-, linear-, and cubic-scaling increases with time as is shown in figure 3–2C and shows the continuous nature of the linear- and cubic scaled drainage discharge and that all three approaches result in the same drain discharge rate when the relative drain head difference is greater than or equal to one. Figure 3–2D shows that the cumulative drain discharge for the original drain formulation is 170 to 200  $L^3$  greater than the cubic- and linear-scaled drainage discharge, respectively.

### Incorporation of the modified Drain (DRN) Package into the CVFD Groundwater Flow Equation

To prepare the CVFD equation for solution using the standard formulation, it is convenient to rearrange the discretized groundwater flow equation for a cell so that all terms containing heads at the end of the current time step are grouped on the left-hand side of the equation, and all terms that are independent of head at the end of the current time step are on the right-hand side of equation 6–1 in [Langevin and others \(2017\)](#). Refer to [Langevin and others \(2017\)](#) for additional information on how the groundwater flow equation is formulated in MODFLOW 6.

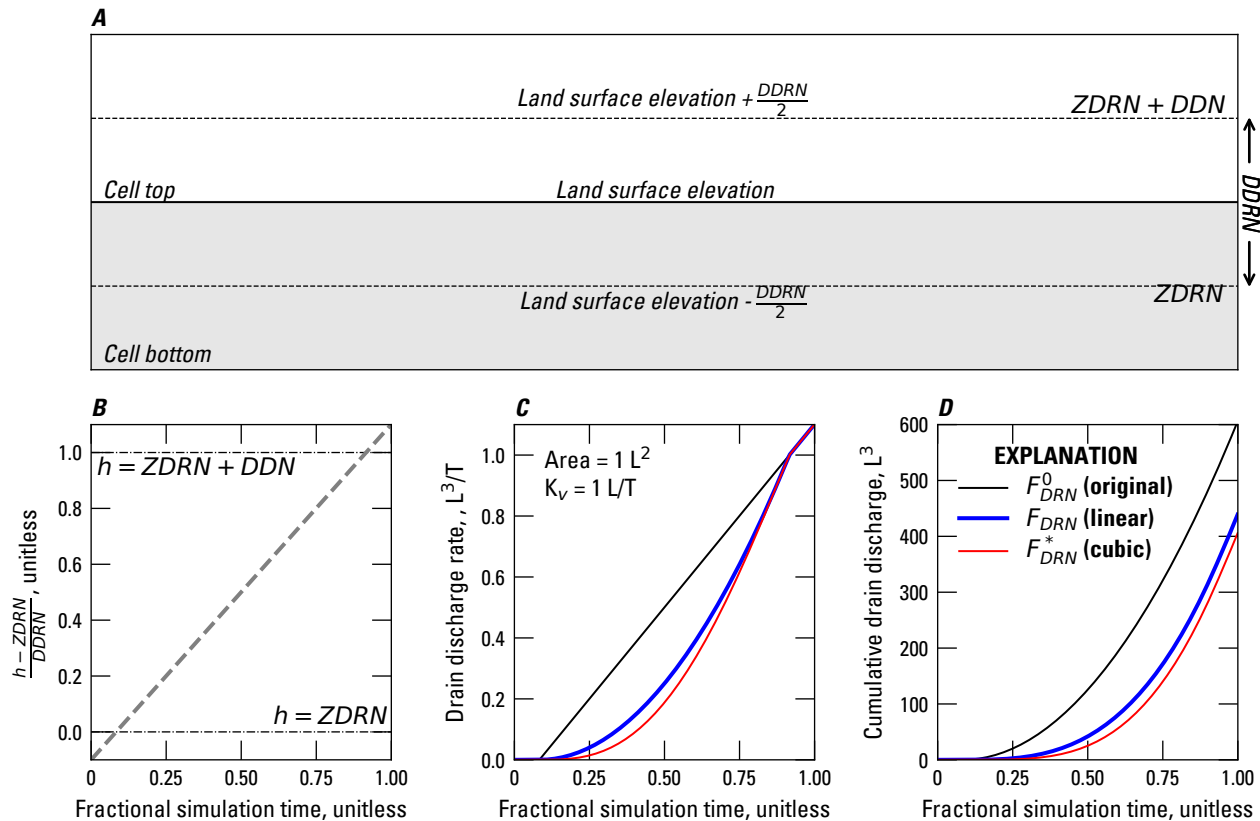


**Figure 3–2.** Graphs showing a conceptual model cell using scaled drain discharge and the relation between the groundwater level and drain discharge. **A**, Conceptual model cell containing a drain cell where drainage discharge starts  $\frac{DDRN}{2}$  below land surface and is equal  $\frac{DDRN}{2}$  above land surface for all drain scaling approaches, **B**, conceptual linear groundwater level increases, which are presented as a relative drain head difference, with fractional simulation time, **C**, calculated original, linear, and cubic scaled drainage discharge rates resulting from conceptual groundwater level increases, and **D**, calculated original, linear, and cubic scaled drainage cumulative discharge resulting from conceptual groundwater level increases.

## Standard Formulation

According to the sign convention in MODFLOW 6,  $QDRN_{nb}$  in the groundwater flow equation is defined as a head-dependent flow out of cell  $n$ , and corresponding terms must be added to the left and right sides of equation 6–1 in Langevin and others (2017) for each cell containing a drain. This is accomplished in the modified Drain Package by adding the head-dependent term and the known term in equation 3–3 to the left- and right-side of equation 6–1 in Langevin and others (2017). The contribution of the modified drain equations to the left-hand side and right-hand sides of the groundwater flow equation are

$$\begin{aligned} A_{n,n} &\leftarrow A_{n,n} - F_{DRN_{nb}} CDRN_{nb} \\ b_n &\leftarrow b_n - F_{DRN_{nb}} CDRN_{nb} ZDRN_{nb}, \end{aligned} \quad (3-15)$$

where  $A_{n,n}$  is the diagonal of the coefficient matrix for cell  $n$  and  $b_n$  is the right-hand side of the groundwater flow equation for cell  $n$ . In the case where drainage discharge is not scaled,  $F_{DRN_{nb}}$  is zero when  $h_n$  is less than or equal to  $HDRN_{nb}$  and one when  $h_n$  is greater than  $HDRN_{nb}$ , which results in identical behavior as the original drain package formulation.

## 3–6 MODFLOW 6 – Supplemental Technical Information

### Newton-Raphson Formulation

The modified Newton-Raphson form of equation 3–10 solved in terms of  $h$  instead of  $\Delta h$  and incorporated into the Newton-Raphson form of the groundwater flow equation (Langevin and others, 2017, eq. 2–26) is

$$\frac{\partial QDRN_{nb}^*}{\partial h_n} h_n^k = -QDRN_{nb}^* + \frac{\partial QDRN_{nb}^*}{\partial h_n} h_n^{k-1}, \quad (3-16)$$

where  $h_n^k$  is the head at the end of the current non-linear (picard) iteration and  $h_n^{k-1}$  is the head at the start of the current non-linear iteration. Substitution of equations 3–10 and 3–13 into equation 3–16 results in

$$\begin{aligned} A_{n,n} &\leftarrow A_{n,n} - F_{DRN_{nb}}^* CDRN_{nb} + \frac{\partial F_{DRN_{nb}}^*}{\partial h} CDRN_{nb} (ZDRN_{nb} - h_n) \\ b_n &\leftarrow b_n - F_{DRN_{nb}}^* CDRN_{nb} (ZDRN_{nb} - h_n^{k-1}) \\ &+ \left[ -F_{DRN_{nb}}^* CDRN_{nb} + \frac{\partial F_{DRN_{nb}}^*}{\partial h} CDRN_{nb} (ZDRN_{nb} - h_n) \right] h_n^{k-1}. \end{aligned} \quad (3-17)$$

Simplifying the right-hand side contribution in equation 3–17 results in

$$b_n \leftarrow b_n - F_{DRN_{nb}}^* CDRN_{nb} ZDRN_{nb} + \left[ \frac{\partial F_{DRN_{nb}}^*}{\partial h} CDRN_{nb} (ZDRN_{nb} - h_n) \right] h_n^{k-1}. \quad (3-18)$$

The  $F_{DRN_{nb}}^* CDRN_{nb}$  term in equation 3–17 and the  $F_{DRN_{nb}}^* CDRN_{nb} ZDRN_{nb}$  term in equation 3–18 are subtracted from the diagonal of the coefficient matrix and the right-hand side of the groundwater-flow equation, respectively, during the standard formulation step for the drain package. The Newton-Raphson formulation for the modified drain package is completed by augmenting the coefficient matrix with the derivative term in equation 3–17 and adding the second term in equation 3–18 (the product of a derivative term and the head at the start of the current iteration) to the right-hand side of the groundwater-flow equation.

### Use of Drain Discharge Scaling

A few examples of how the modified drain package can be used to simulate drainage discharge consistent with other MODFLOW 6 packages are given below.

#### The original drain package formulation with a specified drainage depth value

Specifying  $DDRN$  to be 0 results in a drain that behaves the same as the original DRN Package (eq. 3–1). Using a combination of  $DDRN$  values set to zero and non-zero values will result in drains with 0 values behaving like the original drain package and others using the scaled drainage discharge approach.

#### Groundwater seepage from the Unsaturated Zone Flow Package

The drain package can be used as an alternative to the groundwater seepage option in the Unsaturated Zone Flow (UZF) Package. Specifying a positive  $DDRN$  value and  $HDRN_{nb}$  to be  $\frac{DDRN}{2}$  below the single values specified with the standard DRN Package approach (for example, setting  $DDRN$  to be at land surface) results in a formulation that is equivalent to the groundwater seepage option available in the UZF Package in

MODFLOW 6 ([Langevin and others, 2017](#)). To be consistent with the UZF package, the drain conductance should be calculated as

$$CDRN_{nb} = \frac{K_{v_{nb}} A_n}{DDRN_{nb}}, \quad (3-19)$$

where  $K_{v_{nb}}$  is vertical hydraulic conductivity ( $LT^{-1}$ ) and  $A_n$  is the horizontal area of cell  $n$  ( $L^2$ ).

## Chapter 4. Multi-Aquifer Well Package Connection Flow Correction

Special considerations are required for flow to convertible cells that can dry and rewet. When flow is between two cells that are wet, the head difference between them creates the driving force for flow. When the downstream cell is dry, however, a reference elevation can be used instead of the downstream head to express flow between the nodes. The “perched” option in the Node Property Flow (NPF) Package can be used to correct downward flow to a partially saturated cell.

The “flow correction” option in the Multi-Aquifer Well (MAW) Package implements the same correction as the NPF package “perched” option and corrects the flow between a multi-aquifer well connection and a GWF cell. The approach used in the MAW Package is identical to the “flow-to-dry-cell” option available in MODFLOW-USG ([Panday and others, 2013](#)).

### Multi-Aquifer Well Flow Correction

When the “flow correction” option is enabled, flow to a well from a GWF cell based on equation 7–50 in [Langevin and others \(2017\)](#) is

$$Q_{MAW,MAW,n} = \begin{cases} S_{MAW,n} C_{MAW,n}^0 (h_n - e_{MAW,n}) & HMAW_i < e_{MAW,n}, \\ S_{MAW,n} C_{MAW,n}^0 (h_n - HMAW_i) & HMAW_i \geq e_{MAW,n}, \end{cases} \quad (4-1)$$

where  $S_{MAW,n}$  is the well screen saturation (unitless),  $C_{MAW,n}^0$  is the saturated well conductance ( $L^2 T^{-1}$ ),  $h_n$  is the head in cell  $n$  ( $L$ ),  $e_{MAW,n}$  is the reference elevation for the well connection ( $L$ ), and  $HMAW_i$  is the head in well  $i$  ( $L$ ). The reference elevation for the well connection is defined to be

$$e_{MAW,n} = \begin{cases} BOT_n & BOT_n > BOT_{MAW,n}, \\ BOT_{MAW,n} & BOT_{MAW,n} > BOT_n, \end{cases} \quad (4-2)$$

where  $BOT_n$  is the bottom of cell  $n$  ( $L$ ) and  $BOT_{MAW,n}$  is the bottom of the well screen for the connection of well  $i$  to cell  $n$  ( $L$ ). For the case where the head in cell  $n$  is less than  $e_{MAW,n}$ , flow from a well to a GWF cell is

$$Q_{MAW,MAW,n} = \begin{cases} S_{MAW,n} C_{MAW,n}^0 (e_{MAW,n} - HMAW_i) & h_n < e_{MAW,n}, \\ S_{MAW,n} C_{MAW,n}^0 (h_n - HMAW_i) & h_n \geq e_{MAW,n}. \end{cases} \quad (4-3)$$

### Incorporation of the Flow Correction into the CVFD Groundwater Flow Equation

Multi-aquifer well flow terms are incorporated into the CVFD flow equation ([Langevin and others, 2017](#), eq. 6–1) based on whether the standard or Newton-Raphson formulation is being used. The details of how the multi-aquifer well flow correction terms are incorporated into the CVFD flow equation is described below.

#### Standard Formulation

The terms in the standard flow equation for all groundwater cells connected to a multi-aquifer well  $i$  based on ([Langevin and others, 2017](#), eq. 7–55) is

## 4–2 MODFLOW 6 – Supplemental Technical Information

$$\sum_{n \in MAW_i} S_{MAW,n} C_{MAW,n}^0 (h_n - HMAW_i) = 0. \quad (4-4)$$

To implement the flow correction, equation 4–1 is modified to

$$QMAW_{MAW,n} = S_{MAW,n} C_{MAW,n}^0 (h_n - HMAW_i) + S_{MAW,n} C_{MAW,n}^0 (HMAW_i - \bar{h}_{MAW,n}), \quad (4-5)$$

where  $\bar{h}_{MAW,n}$  is a function that transitions between the head at the downstream node,  $HMAW_i$  in this case, and reference elevation  $e_{MAW,n}$ . The downstream head transition function used to correct the multi-aquifer flow for a connection is calculated as

$$\bar{h}_{MAW,n} = \begin{cases} e_{MAW,n} & h_{ds} < e_{MAW,n}, \\ h_{ds} & h_{ds} \geq e_{MAW,n} \end{cases}, \quad (4-6)$$

where  $h_{ds}$  is head in the downstream node ( $L$ ), which is the minimum of  $HMAW_i$  and  $h_n$ . The relation between the downstream head and  $\bar{h}_{MAW,n}$  is shown in figure 4–1.

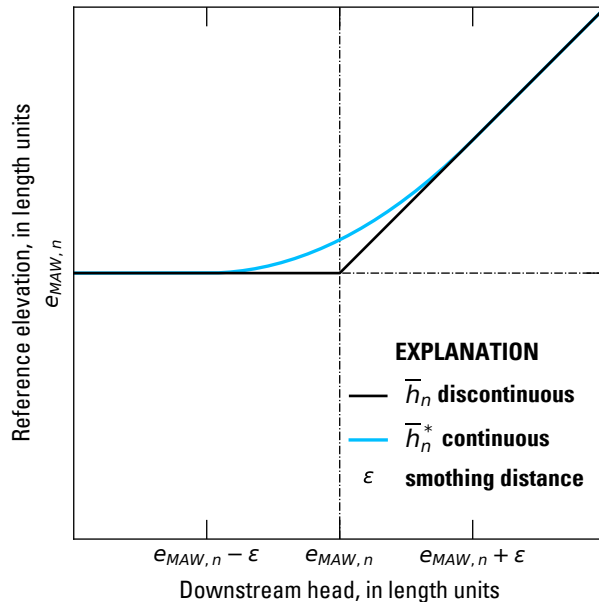


**Figure 4–1.** Graph showing the discontinuous (eq. 4–6) and continuous (eq. 4–9) downstream head transition function used to correct the multi-aquifer flow for a connection as it transitions from saturated to partially saturated conditions. The interval over which the smoothing occurs,  $\epsilon$ , is also shown.

Similarly, when  $h_n$  is the downstream node equation 4–3 is modified to

$$QMAW_{MAW,n} = S_{MAW,n} C_{MAW,n}^0 (h_n - HMAW_i) + S_{MAW,n} C_{MAW,n}^0 (\bar{h}_{MAW,n} - h_n), \quad (4-7)$$

The first term on the right hand side of equations 4-5 and 4-7 ( $S_{MAW,n}C_{MAW,n}^0$ ) are added to the coefficient matrix used to solve the coupled groundwater and multi-aquifer well flow equations as part of the standard MAW package formulation (Langevin and others, 2017, eq. 7-55). The flow correction is made by subtracting the second term on the right hand side of equations 4-5 and 4-7 from the right had side of equation 6-1 in Langevin and others (2017). In the case where  $HMAW_i$  and  $h_n$  are both greater than  $e_{MAW,n}$ , the second term on the right hand side of equations 4-5 and 4-7 is equal to zero, which results in a equation identical to equation 4-4 for a single connection.

## Newton-Raphson Formulation

The modified Newton-Raphson form of equation 4-4 solved for a single connection in terms of  $h$  instead of  $\Delta h$  and incorporated into the Newton-Raphson form of the groundwater flow equation (Langevin and others, 2017, eq. 2-26) is

$$\frac{\partial QMAW_{MAW,n}}{\partial HMAW_i} HMAW_i^k + \frac{\partial QMAW_{MAW,n}}{\partial h_n} h_n^k = -QMAW_{MAW,n} + \frac{\partial QMAW_{MAW,n}}{\partial HMAW_i} HMAW_i^{k-1} + \frac{\partial QMAW_{MAW,n}}{\partial h_n} h_n^{k-1}, \quad (4-8)$$

where  $HMAW_i^k$  and  $h_n^k$  are the heads at the end of the current non-linear (picard) iteration and  $HMAW_i^{k-1}$  and  $h_n^{k-1}$  are the head at the start of the current non-linear iteration.

When the Newton-Raphson formulation is used, discontinuous derivatives can cause non-convergence in the neighborhood of the discontinuity (Kavetski and Kuczera, 2007). As a result, the discontinuous well screen saturation ( $S_{MAW,n}$ ) in equations 4-5 and 4-7 is replaced by a quadratically smoothed well screen saturation ( $S_{MAW,n}^*$  – eq. 4-5 in Langevin and others (2017)). The discontinuous downstream head transition function ( $\bar{h}_{MAW,n}$ , eq. 4-6) in equations 4-5 and 4-7 is also replaced by

$$\bar{h}_{MAW,n}^* = \begin{cases} e_{MAW,n} & h_{ds} - e_{MAW,n} < -\epsilon \\ \frac{(h_{ds} - e_{MAW,n})^2}{4\epsilon} + \frac{(h_{ds} - e_{MAW,n})}{2} + \frac{\epsilon}{4} + e_{MAW,n} & -\epsilon < h_{ds} - e_{MAW,n} < +\epsilon \\ h_{ds} & h_{ds} - e_{MAW,n} \geq +\epsilon \end{cases} \quad (4-9)$$

where  $\epsilon$  is the interval over which the head transition function is smoothed. The relation between the downstream head and  $\bar{h}_{MAW,n}^*$  is shown in figure 4-1. Simplification of equations 4-5 and 4-7 results in

$$QMAW_{MAW,n} = S_{MAW,n}^* C_{MAW,n}^0 (h_n - \bar{h}_{MAW,n}^*) \quad (4-10)$$

and

$$QMAW_{MAW,n} = S_{MAW,n}^* C_{MAW,n}^0 (\bar{h}_{MAW,n}^* - HMAW_i) \quad (4-11)$$

when  $HMAW_i$  and  $h_n$  are the downstream heads, respectively. The derivatives of equation 4-10 with respect to  $h_n$  and  $HMAW_i$  are

#### 4-4 MODFLOW 6 – Supplemental Technical Information

$$\frac{\partial Q_{MAW}}{\partial HMAW_i} = -S_{MAW,n}^* C_{MAW,n}^0 \frac{\partial \bar{h}_{MAW,n}^*}{\partial HMAW_i} \quad (4-12)$$

and

$$\frac{\partial Q_{MAW}}{\partial h_n} = S_{MAW,n}^* C_{MAW,n}^0 + \frac{\partial S_{MAW,n}^*}{\partial h_n} C_{MAW,n}^0 (h_n - \bar{h}_{MAW,n}^*), \quad (4-13)$$

respectively. The derivatives of equation 4-11 with respect to  $h_n$  and  $HMAW_i$  are

$$\frac{\partial Q_{MAW}}{\partial HMAW_i} = -S_{MAW,n}^* C_{MAW,n}^0 + \frac{\partial S_{MAW,n}^*}{\partial HMAW_i} C_{MAW,n}^0 (\bar{h}_{MAW,n}^* - HMAW_i) \quad (4-14)$$

and

$$\frac{\partial Q_{MAW}}{\partial h_n} = S_{MAW,n}^* C_{MAW,n}^0 \frac{\partial \bar{h}_{MAW,n}^*}{\partial h_n}. \quad (4-15)$$

The derivative of  $\bar{h}_{MAW,n}^*$  with respect to the downstream head is

$$\frac{\partial \bar{h}_{MAW,n}^*}{\partial h_{ds}} = \begin{cases} 0 & h_{ds} - e_{MAW,n} < -\epsilon \\ \frac{h_{ds} - e_{MAW,n}}{2\epsilon} + \frac{1}{2} & -\epsilon < h_{ds} - e_{MAW,n} < +\epsilon \\ 1 & h_{ds} - e_{MAW,n} \geq +\epsilon \end{cases} \quad (4-16)$$

#### Newton-Raphson formulation when $HMAW_i$ is the Downstream Head

The Newton-Raphson form of the equation 4-5, when  $HMAW_i$  is the downstream head, is formulated by substituting equations 4-10, 4-12, and 4-13 into equation 4-8, which results in

$$\begin{aligned} & \left[ -S_{MAW,n}^* C_{MAW,n}^0 \frac{\partial \bar{h}_{MAW,n}^*}{\partial HMAW_i} \right] HMAW_i^k + \\ & \left[ S_{MAW,n}^* C_{MAW,n}^0 + \frac{\partial S_{MAW,n}^*}{\partial h_n} C_{MAW,n}^0 (h_n^{k-1} - \bar{h}_{MAW,n}^{k-1}) \right] h_n^k = \\ & -S_{MAW,n}^* C_{MAW,n}^0 (h_n^{k-1} - \bar{h}_{MAW,n}^{k-1}) + \\ & \left[ -S_{MAW,n}^* C_{MAW,n}^0 \frac{\partial \bar{h}_{MAW,n}^*}{\partial HMAW_i} \right] HMAW_i^{k-1} + \\ & \left[ S_{MAW,n}^* C_{MAW,n}^0 + \frac{\partial S_{MAW,n}^*}{\partial h_n} C_{MAW,n}^0 (h_n^{k-1} - \bar{h}_{MAW,n}^{k-1}) \right] h_n^{k-1}. \end{aligned} \quad (4-17)$$

Simplifying equation 4-17 results in

$$\begin{aligned}
 & \left[ -S_{MAW,n}^* C_{MAW,n}^0 \frac{\partial \bar{h}_{MAW,n}^*}{\partial HMAW_i} \right] HMAW_i^k + \\
 & \left[ S_{MAW,n}^* C_{MAW,n}^0 + \frac{\partial S_{MAW,n}^*}{\partial h_n} C_{MAW,n}^0 (h_n^{k-1} - \bar{h}_{MAW,n}^{*k-1}) \right] h_n^k = \\
 & S_{MAW,n}^* C_{MAW,n}^0 \bar{h}_{MAW,n}^{*k-1} + \left[ -S_{MAW,n}^* C_{MAW,n}^0 \frac{\partial \bar{h}_{MAW,n}^*}{\partial HMAW_i} \right] HMAW_i^{k-1} + \\
 & \left[ \frac{\partial S_{MAW,n}^*}{\partial h_n} C_{MAW,n}^0 (h_n^{k-1} - \bar{h}_{MAW,n}^{*k-1}) \right] h_n^{k-1}.
 \end{aligned} \tag{4-18}$$

To complete the Newton-Raphson formulation the terms added to the coefficient matrix and right-hand side during the standard formulation step (eq. 4-5) are modified by adding

$$S_{MAW,n}^* C_{MAW,n}^0 \left( 1 - \frac{\partial \bar{h}_{MAW,n}^*}{\partial HMAW_i} \right) \tag{4-19}$$

to the diagonal position in the row for multi-aquifer well  $i$ , adding

$$\frac{\partial S_{MAW,n}^*}{\partial h_n} C_{MAW,n}^0 (h_n - \bar{h}_{MAW,n}^*) \tag{4-20}$$

to the off-diagonal position for GWF cell  $n$  in the row for multi-aquifer well  $i$ , and adding

$$S_{MAW,n}^* C_{MAW,n}^0 \left( 1 - \frac{\partial \bar{h}_{MAW,n}^*}{\partial HMAW_i} \right) HMAW_i^{k-1} + \frac{\partial S_{MAW,n}^*}{\partial h_n} C_{MAW,n}^0 (h_n - \bar{h}_{MAW,n}^*) h_n^{k-1} \tag{4-21}$$

to the right-hand side in the row for multi-aquifer well  $i$ . The  $\left( 1 - \frac{\partial \bar{h}_{MAW,n}^*}{\partial HMAW_i} \right)$  term in equation 4-19 removes the  $-S_{MAW,n}^* C_{MAW,n}^0$  term added during standard formulation step and correctly adds the  $-S_{MAW,n}^* C_{MAW,n}^0 \frac{\partial \bar{h}_{MAW,n}^*}{\partial HMAW_i}$  term. The row for the connected groundwater cell (row  $n$ ) is also modified by subtracting equations 4-19, 4-20, and 4-21 from the off-diagonal (column corresponding to multi-aquifer well  $i$ ), diagonal, and right-hand side, respectively.

#### Newton-Raphson formulation when $h_n$ is the Downstream Head

The Newton-Raphson form of the equation 4-7, when  $h_n$  is the downstream head, is formulated by substituting equations 4-11, 4-14, and 4-15 into equation 4-8, which results in

## 4–6 MODFLOW 6 – Supplemental Technical Information

$$\begin{aligned}
& \left[ -S_{MAW,n}^* C_{MAW,n}^0 + \frac{\partial S_{MAW,n}^*}{\partial HMAW_i} C_{MAW,n}^0 (\bar{h}_{MAW,n}^{*k-1} - HMAW_i^{k-1}) \right] HMAW_i^k + \\
& \left[ S_{MAW,n}^* C_{MAW,n}^0 \frac{\partial \bar{h}_{MAW,n}^*}{\partial h_n} \right] h_n^k = -S_{MAW,n}^* C_{MAW,n}^0 (\bar{h}_{MAW,n}^{*k-1} - HMAW_i^{k-1}) + \\
& \left[ -S_{MAW,n}^* C_{MAW,n}^0 + \frac{\partial S_{MAW,n}^*}{\partial HMAW_i} C_{MAW,n}^0 (\bar{h}_{MAW,n}^{*k-1} - HMAW_i^{k-1}) \right] HMAW_i^{k-1} + \\
& \left[ S_{MAW,n}^* C_{MAW,n}^0 \frac{\partial \bar{h}_{MAW,n}^*}{\partial h_n} \right] h_n^{k-1}.
\end{aligned} \tag{4-22}$$

Simplifying equation 4-22 results in

$$\begin{aligned}
& \left[ -S_{MAW,n}^* C_{MAW,n}^0 + \frac{\partial S_{MAW,n}^*}{\partial HMAW_i} C_{MAW,n}^0 (\bar{h}_{MAW,n}^{*k-1} - HMAW_i^{k-1}) \right] HMAW_i^k + \\
& \left[ S_{MAW,n}^* C_{MAW,n}^0 \frac{\partial \bar{h}_{MAW,n}^*}{\partial h_n} \right] h_n^k = -S_{MAW,n}^* C_{MAW,n}^0 \bar{h}_{MAW,n}^{*k-1} + \\
& \left[ \frac{\partial S_{MAW,n}^*}{\partial HMAW_i} C_{MAW,n}^0 (\bar{h}_{MAW,n}^{*k-1} - HMAW_i^{k-1}) \right] HMAW_i^{k-1} + \\
& \left[ S_{MAW,n}^* C_{MAW,n}^0 \frac{\partial \bar{h}_{MAW,n}^*}{\partial h_n} \right] h_n^{k-1}.
\end{aligned} \tag{4-23}$$

To complete the Newton-Raphson formulation the terms added to the coefficient matrix and right-hand side during the standard formulation step (eq. 4-7) are modified by adding

$$\frac{\partial S_{MAW,n}^*}{\partial HMAW_i} C_{MAW,n}^0 (\bar{h}_{MAW,n}^{*k-1} - HMAW_i^{k-1}) \tag{4-24}$$

to the diagonal position in the row for multi-aquifer well  $i$ , adding

$$S_{MAW,n}^* C_{MAW,n}^0 \left( \frac{\partial \bar{h}_{MAW,n}^*}{\partial h_n} - 1 \right) \tag{4-25}$$

to the off-diagonal position for GWF cell  $n$  in the row for multi-aquifer well  $i$ , and adding

$$\frac{\partial S_{MAW,n}^*}{\partial HMAW_i} C_{MAW,n}^0 (\bar{h}_{MAW,n}^{*k-1} - HMAW_i^{k-1}) HMAW_i^{k-1} + S_{MAW,n}^* C_{MAW,n}^0 \left( \frac{\partial \bar{h}_{MAW,n}^*}{\partial h_n} - 1 \right) h_n^{k-1} \tag{4-26}$$

to the right-hand side in the row for multi-aquifer well  $i$ . The  $\left( \frac{\partial \bar{h}_{MAW,n}^*}{\partial h_n} - 1 \right)$  term in equation 4-25 removes the  $S_{MAW,n}^* C_{MAW,n}^0$  term added during standard formulation step and correctly adds the

$S_{MAW,n}^* C_{MAW,n}^0 \frac{\partial \bar{h}_{MAW,n}^*}{\partial h_n}$  term. The row for the connected groundwater cell (row  $n$ ) is also modified by subtracting equations 4-24, 4-25, and 4-26 from the off-diagonal (column corresponding to multi-aquifer well  $i$ ), diagonal, and right-hand side, respectively.

## Chapter 5. Storage Package Modifications

The MODFLOW 6 Storage (STO) Package simulates the contributions of specific storage and specific yield to the groundwater flow equations. Under confined conditions, in which the head above the top of the cell, storage changes are attributable solely to specific storage. Under unconfined conditions, in which the head is above the bottom but below the top of the cell, storage changes are attributable primarily to specific yield, but the contribution of specific storage is also taken into account.

In the original release of the MODFLOW 6 STO Package, the contribution of specific yield is formulated in terms of hydraulic head in a way that conserves water volume but renders the storage change under unconfined conditions dependent on the vertical datum relative to which heads and elevations are defined. Reexamination of the specific storage contribution in terms of pressure head leads to a revised formulation that eliminates the vertical datum dependence and still honors water conservation. This chapter describes the revised specific storage formulation used in the MODFLOW 6 STO Package.

### Original Approach

The specific storage formulation used prior to MODFLOW 6 version 6.1.3 is

$$Q_{SS} = \frac{SC1}{\Delta t} \left( S_F^{t_{old}} h^{t_{old}} - S_F^t h^t \right), \quad (5-1)$$

where  $Q_{SS}$  is the volumetric flow rate from specific storage in the cell ( $L^3/T$ ),  $SC1$  is the primary storage coefficient ( $L^2$ ),  $\Delta t = t - t_{old}$  is the time step length ( $T$ ),  $S_F$  is the fractional saturation of the cell for the previous ( $t_{old}$ ) or current ( $t$ ) time step (unitless),  $h$  is the head in the cell for the previous ( $t_{old}$ ) or current ( $t$ ) time step ( $L$ ). The subscript that indicates the cell number has been omitted for clarity. The primary storage coefficient is calculated as

$$SC1 = S_s A \Delta z, \quad (5-2)$$

where  $S_s$  is the specific storage coefficient for the cell ( $L^{-1}$ ),  $A$  is the horizontal area of the cell ( $L^2$ ), and  $\Delta z$  is the cell thickness ( $L$ ) defined by

$$\Delta z = TOP - BOT, \quad (5-3)$$

where  $TOP$  and  $BOT$  are the top and bottom elevations ( $L$ ) of the cell, respectively. The cell saturation is related to the head in the cell by

$$S_F = \begin{cases} 1 & h > TOP \\ \frac{h - BOT}{\Delta z} & BOT < h \leq TOP \\ 0 & h \leq BOT \end{cases}. \quad (5-4)$$

When the Newton-Raphson formulation is used, the cell saturation in equation 5-4 is quadratically smoothed to provide a continuous derivative with respect to head (see [Langevin and others, 2017](#), Fig. 4-1 and Eq. 4-5).

The cell saturation was included in equation 5-1 to scale the primary storage coefficient in proportion to the saturated volume of water in the cell under water-table conditions. However, the formulation in equa-

## 5–2 MODFLOW 6 – Supplemental Technical Information

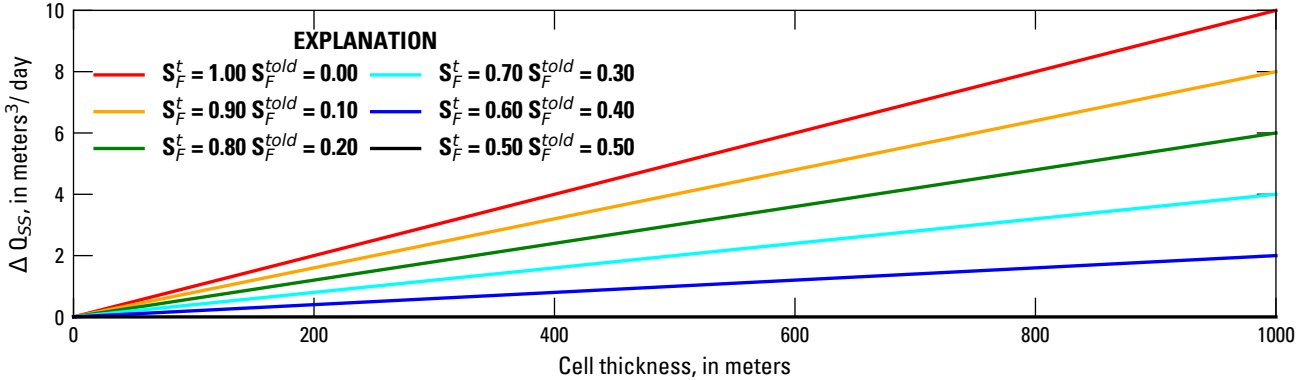


**Figure 5–1.** Graph showing changes in the flow from specific storage,  $Q_{SS}$ , that result from changing the vertical datum from 0 to 1,000 m. The change in  $Q_{SS}$  is plotted at a function of cell thickness,  $\Delta z$ , for various combinations of initial and final cell saturations,  $S_F^{told}$  and  $S_F^t$ . In this example,  $S_s = 1 \times 10^{-5} \text{ m}^{-1}$ ,  $A = 1 \text{ m}^2$ , and  $\Delta t = 1 \text{ d}$ .

tion 5–1 causes the calculated value of  $Q_{SS}$  to depend on the vertical datum, or reference elevation, relative to which heads and elevations are defined. If the vertical datum is changed by an amount  $\Delta z_{ref}$  ( $L$ ), all head values change by an amount  $-\Delta z_{ref}$ , and equation 5–1 becomes

$$Q_{SS} = \frac{SC1}{\Delta t} \left[ S_F^{told} (h^{told} - \Delta z_{ref}) - S_F^t (h^t - \Delta z_{ref}) \right], \quad (5–5)$$

Comparison of equations 5–1 and 5–5 shows that changing the vertical datum by  $\Delta z_{ref}$  changes the calculated value of  $Q_{SS}$  by

$$\Delta Q_{SS} = \frac{SC1}{\Delta t} \left( S_F^{told} - S_F^t \right) \Delta z_{ref}, \quad (5–6)$$

Dependence of  $Q_{SS}$  on the vertical datum is not physically realistic and introduces error into the calculated value of  $Q_{SS}$ . To illustrate the magnitude of the error that can be introduced, equations 5–6 and 5–2 were used to calculate  $\Delta Q_{SS}$  for a range of cell saturations at times  $t$  and  $t_{old}$  and cell thicknesses (fig. 5–1). For this example, a specific storage value of  $1 \times 10^{-5} \text{ m}^{-1}$ , a cell area of  $1 \text{ m}^2$ , and a time step length of 1 d was used in all of the calculations.  $\Delta Q_{SS}$  increases as the cell thickness increases or the difference in cell saturations at times  $t$  and  $t_{old}$  increases.

A related deficiency of equation 5–1 concerns when a cell is dry either at the beginning ( $S_F^{told} = 0$ ) or the end ( $S_F^t = 0$ ) of a time step, in which case the volumetric flow from specific storage equals

$$Q_{SS} = \begin{cases} \frac{SC1}{\Delta t} S_F^{told} h^{told} & S_F^t = 0 \\ -\frac{SC1}{\Delta t} S_F^t h^t & S_F^{told} = 0 \end{cases}. \quad (5–7)$$

Equation 5–7 can overestimate or underestimate the volumetric flow from specific storage, depending on the values of  $h^{told}$  and  $h^t$ , which in turn depend on the vertical datum. For example, in the case of a cell going dry ( $S_F^{told} > 0$ ,  $S_F^t = 0$ ), water flows from specific storage, which implies  $Q_{SS}$  is positive in sign. Because the cell is initially not dry, the initial cell head,  $h^{told}$ , is above the cell bottom elevation. However, depending on the vertical datum, it is possible that  $h^{told}$  is negative in sign (with the cell bottom elevation being even more neg-

ative). In that case, equation 5-7 calculates a negative value for  $Q_{SS}$ , which is opposite to what is expected on physical grounds.

## Revised Formulation

To correct the deficiencies in the original specific storage formulation, the contribution of specific storage to the groundwater flow equation under water-table conditions is reexamined in terms of pressure head, which for a given elevation  $z$  is defined as

$$\psi = h - z. \quad (5-8)$$

The hydraulic head,  $h$ , associated with a MODFLOW cell is formally assigned to a point in the cell called the node, which under water-table conditions is at an elevation halfway between the cell bottom and the water table. The water-table elevation is, in turn, equal to the cell head,  $h$ . Thus, the value of the hydraulic head is the same at the node as it is at the water table, which is consistent with conceptualizing hydraulic head as being constant throughout the saturated portion of the cell. Extending this conceptualization to pressure head via equation 5-8 implies a linear variation of pressure head between a value of 0 at the water table and a value of  $h - BOT$  at the cell bottom. The revised specific storage formulation is therefore based on linear variation of pressure head with elevation within a cell.

The volumetric water content,  $\theta$ , at elevation  $z$  within a cell is related to pressure head by

$$\theta = \begin{cases} \theta_r & z > h \\ S_s\psi + S_y + \theta_r & z \leq h \end{cases}, \quad (5-9)$$

where  $\theta_r$  is the specific retention (unitless) and  $S_y$  is the specific yield (unitless) in the cell. Integration of equation 5-9 from the bottom to the top of the cell gives the total volume of water stored in the cell:

$$V_S = A \int_{BOT}^{TOP} \theta dz = A \int_{BOT}^{z_{wt}^*} S_s\psi dz + A \int_{BOT}^{z_{wt}^*} S_y dz + A \int_{BOT}^{TOP} \theta_r dz, \quad (5-10)$$

where  $z_{wt}^*$  is the water-table elevation limited by the top elevation of the cell, given by

$$z_{wt}^* = BOT + \Delta z S_F. \quad (5-11)$$

Assuming  $\theta_r$ ,  $S_y$ , and  $S_s$  are uniform throughout the cell, substitution of equation 5-8 into equation 5-10 and evaluation of the integrals gives

$$V_S = S_s A \Delta z S_F (h - \bar{z}) + S_y A \Delta z S_F + \theta_r A \Delta z, \quad (5-12)$$

where  $\bar{z}$  is the node elevation (the vertical center of the saturated portion of the cell) given by

$$\bar{z} = \frac{1}{z_{wt}^* - BOT} \int_{BOT}^{z_{wt}^*} z dz = BOT + \frac{\Delta z}{2} S_F. \quad (5-13)$$

## 5–4 MODFLOW 6 – Supplemental Technical Information

The remainder of this chapter focuses on the contribution of specific storage (the first term on the right-hand side of equation 5–12) to the change in storage in a cell during a time step. The contribution of specific yield is calculated separately in MODFLOW 6 and remains unchanged by the revised approach described here. The volume of water in specific retention is assumed to be constant and therefore does not contribute to changes in storage.

Substitution of equations 5–2 and 5–13 into the first term on the right-hand side of equation 5–12 gives the volume of water in compressible storage in the cell,

$$V_{SS} = SC1 S_F \left( h - BOT - \frac{\Delta z}{2} S_F \right). \quad (5-14)$$

The revised volumetric flow rate from compressible storage is then

$$Q_{SS} = \frac{SC1}{\Delta t} \left[ S_F^{t_{old}} \left( h^{t_{old}} - BOT - \frac{\Delta z}{2} S_F^{t_{old}} \right) - S_F^t \left( h^t - BOT - \frac{\Delta z}{2} S_F^t \right) \right]. \quad (5-15)$$

When a cell is fully saturated ( $S_F = 1$ ) at times  $t$  and  $t_{old}$ , equation 5–15 simplifies to

$$Q_{SS} = \frac{SC1}{\Delta t} (h^{t_{old}} - h^t), \quad (5-16)$$

which is identical to the original specific storage formulation under confined conditions in MODFLOW 6 and the specific storage formulation under both confined and unconfined conditions in MODFLOW-2005 (Harbaugh, 2005).

The revised formulation in equation 5–15 is no longer dependent on the vertical datum because it involves cell saturations,  $S_F$ , and head differences of the form  $h - BOT$ , which do not change when the vertical datum changes. In the case of a cell being dry either at the beginning or the end of a time step, the volumetric flow from specific storage based on the revised formulation equals

$$Q_{SS} = \begin{cases} \frac{SC1}{\Delta t} S_F^{t_{old}} \left( h^{t_{old}} - BOT - \frac{\Delta z}{2} S_F^{t_{old}} \right) & S_F^t = 0 \\ -\frac{SC1}{\Delta t} S_F^t \left( h^t - BOT - \frac{\Delta z}{2} S_F^t \right) & S_F^{t_{old}} = 0 \end{cases}, \quad (5-17)$$

which is the revised-formulation counterpart of equation 5–7. It can be deduced from equation 5–4 that

$$h - BOT - \frac{\Delta z}{2} S_F > 0 \quad \text{if } h > BOT, \quad (5-18)$$

which implies that equation 5–17 calculates the correct sign for  $Q_{SS}$  when a cell goes dry or resaturates.

## Incorporation of the Revised Specific Storage Formulation into the CVFD Groundwater Flow Equation

The approaches used to incorporate the contribution from specific storage into the linear matrix problem that represents the discretized groundwater flow equation are detailed below. When the standard formulation is used, the cell saturation defined in equation 5–4 is used without modification. To allow for a smooth transition

from dry (water level at or below the bottom of a cell) to fully saturated (water level at or above the top of the cell) conditions when the Newton formulation is used, quadratic smoothing is applied to the cell saturation over a small interval when the water level approaches the top or bottom of a cell, as described in Eq. 4–5 in [Langevin and others \(2017\)](#).

## Standard Formulation

Adding the cell number subscript “ $n$ ” to cellwise quantities in equation [5–15](#) and adding specific storage terms dependent on the current value of head and known terms to the left- and right-hand sides of the discretized groundwater flow equation ([Langevin and others, 2017](#), eq. 6–1), respectively, results in

$$\begin{aligned} A_{n,n} &\leftarrow A_{n,n} - \frac{SC1_n}{\Delta t} S_{F_n}^{k-1} \\ b_n &\leftarrow b_n - \frac{SC1_n}{\Delta t} \left[ S_{F_n}^{t_{old}} \left( h_n^{t_{old}} - BOT_n - \frac{\Delta z_n}{2} S_{F_n}^{t_{old}} \right) + S_{F_n}^{k-1} \left( BOT_n + \frac{\Delta z_n}{2} S_{F_n}^{k-1} \right) \right], \end{aligned} \quad (5–19)$$

where  $A_{n,n}$  is the diagonal of the coefficient matrix for cell  $n$  and  $b_n$  is the right-hand side of the groundwater flow equation for cell  $n$ . A variant of equation [5–19](#) that tries to take advantage of the fact that

$$h_n - BOT_n - \frac{\Delta z_n}{2} S_{F_n} = \frac{1}{2} (h_n - BOT_n) \quad (5–20)$$

under water-table conditions (head in the cell below the top of the cell) was also evaluated. However, the form presented in equation [5–19](#) was found to converge better for the test problems evaluated and to simplify the additional terms added to the left- and right-hand sides of the discretized groundwater equation to complete the Newton-Raphson formulation.

## Newton-Raphson Formulation

Adding the cell number subscript “ $n$ ” to cellwise quantities in equation [5–15](#) and rearranging the equation to facilitate differentiation with respect to the current value of head,  $h_n^t$ , results in

$$Q_{SS_n} = \frac{SC1_n}{\Delta t} \left[ S_{F_n}^{*t_{old}} \left( h_n^{t_{old}} - BOT_n - \frac{\Delta z_n}{2} S_{F_n}^{t_{old}} \right) - S_{F_n}^{*t} (h_n^t - BOT_n) + \frac{\Delta z_n}{2} (S_{F_n}^{*t})^2 \right], \quad (5–21)$$

where  $S_F^*$  is the quadratically smoothed cell saturation (see [Langevin and others, 2017](#), Eq. 4–5). The derivative of equation [5–21](#) with respect to  $h_n^t$  is

$$\frac{\partial Q_{SS_n}}{\partial h_n} = -\frac{SC1_n}{\Delta t} S_{F_n}^{*t} - \frac{SC1_n}{\Delta t} \frac{\partial S_{F_n}^{*t}}{\partial h_n} (h_n^t - BOT_n) + \frac{SC1_n}{\Delta t} \Delta z_n S_{F_n}^{*t} \frac{\partial S_{F_n}^{*t}}{\partial h_n}, \quad (5–22)$$

where the superscript “ $t$ ” has been omitted from  $h_n^t$  in the derivatives for clarity. The fully implicit form of the Newton-Raphson formulation for the contribution of specific storage in the cell in the form of equation 2–30 in [Langevin and others \(2017\)](#) is

$$\frac{\partial Q_{SS_n}}{\partial h_n} h_n^k = -Q_{SS_n} + \frac{\partial Q_{SS_n}}{\partial h_n} h_n^{k-1}. \quad (5–23)$$

## 5–6 MODFLOW 6 – Supplemental Technical Information

where the superscripts “ $k$ ” and “ $k - 1$ ” indicate quantities evaluated on the current and previous outer iterations of the solution procedure, respectively. Replacement of  $h_n^t$  and  $S_{F_n}^{*t}$  by their previous iterates,  $h_n^{k-1}$  and  $S_{F_n}^{*k-1}$ , in equations 5–21 and 5–22 and substitution of those equations into equation 5–23 results in

$$\begin{aligned} A_{n,n} &\leftarrow A_{n,n} + \left[ -\frac{SC1_n}{\Delta t} S_{F_n}^{*k-1} - \frac{SC1_n}{\Delta t} \frac{\partial S_{F_n}^{*k-1}}{\partial h_n} \left( h_n^{k-1} - BOT_n \right) + \frac{SC1_n}{\Delta t} \Delta z_n S_{F_n}^{k-1} \frac{\partial S_{F_n}^{*k-1}}{\partial h_n} \right] \\ b_n &\leftarrow b_n - \frac{SC1_n}{\Delta t} \left[ S_{F_n}^{*t_{old}} \left( h_n^{t_{old}} - BOT_n - \frac{\Delta z_n}{2} S_{F_n}^{*t_{old}} \right) + S_{F_n}^{*k-1} \left( BOT_n + \frac{\Delta z_n}{2} S_{F_n}^{*k-1} \right) \right] \\ &\quad + \left[ -\frac{SC1_n}{\Delta t} \frac{\partial S_{F_n}^{*k-1}}{\partial h_n} \left( h_n^{k-1} - BOT_n \right) + \frac{SC1_n}{\Delta t} \Delta z_n S_{F_n}^{*k-1} \frac{\partial S_{F_n}^{*k-1}}{\partial h_n} \right] h_n^{k-1}. \end{aligned} \quad (5-24)$$

Comparison of equation 5–24 to equation 5–19 shows that many of the terms in the Newton-Raphson formulation were added as part of the standard formulation. The Newton-Raphson formulation is completed by adding the second and third terms on the right-hand side of equation 5–22 and the product of these terms and the current head to the terms already added to the diagonal of the coefficient matrix and right-hand side by the standard formulation, respectively.

## Chapter 6. Time-Varying Hydraulic Conductivity and Storage

The MODFLOW 6 Time-Varying Hydraulic Conductivity (TVK) and Time-Varying Storage (TVS) packages allow hydraulic conductivity, specific storage and specific yield properties of model cells to be varied transiently throughout a simulation. This can be useful for modeling caved rock, void and spoil in mining applications, or for other physical changes to a system that can reasonably be represented by changing material properties.

Changes are made on a cell-by-cell basis in TVK and TVS package input files by specifying new values for elements of NPF package arrays K, K22 and K33, and STO package arrays SS and SY. New values may be applied at the start of each stress period, or alternatively interpolated via time series to determine new values at each time step. Changes are only made to those model cells explicitly specified in the TVK and TVS package input files; other cells retain their original NPF and STO values. Additionally, a change may be made to a cell's value for one property independently without affecting other property values at the same cell, e.g. SS may be changed for a cell without affecting SY, if desired.

Where a property value change is given by a time series, the value continues to change at each time step until the last entry in the time series is reached. Otherwise, once a cell property value has been changed, it remains at its new value until subsequently changed in the TVK or TVS files for a later period, or until the end of the simulation if no further changes are enacted.

By default, when the TVS package is used to change SS or SY values, the MODFLOW 6 storage formulation is modified to integrate these changes such that the head solution correctly reflects changes in pressure due to the corresponding increase or decrease in stored water volume. The modifications are described in the “[Storage Change Integration: Specific Storage](#)” and “[Storage Change Integration: Specific Yield](#)” sections below. If this functionality is not desired, storage change integration may be disabled by activating the DISABLE\_STORAGE\_CHANGE\_INTEGRATION option in the TVS package input file.

### Storage Change Integration: Specific Storage

Revisiting the derivation of the revised storage formulation in the [Storage Package Modifications chapter](#), changes in specific storage are introduced by first separating equation 5–14 into two separate equations:

$$V_{SS}^{t_{old}} = SC1^{t_{old}} S_F^{t_{old}} \left( h^{t_{old}} - BOT - \frac{\Delta z}{2} S_F^{t_{old}} \right), \quad (6-1)$$

giving the volume of water in compressible storage at time  $t_{old}$ , and

$$V_{SS}^t = SC1^t S_F^t \left( h^t - BOT - \frac{\Delta z}{2} S_F^t \right), \quad (6-2)$$

giving the volume of water in compressible storage at time  $t$ . The volumetric flow rate from compressible storage taking into account changes in specific storage is then

$$\begin{aligned} Q_{SS} &= \frac{V_{SS}^{t_{old}} - V_{SS}^t}{\Delta t} \\ &= \frac{SC1^{t_{old}}}{\Delta t} S_F^{t_{old}} \left( h^{t_{old}} - BOT - \frac{\Delta z}{2} S_F^{t_{old}} \right) - \frac{SC1^t}{\Delta t} S_F^t \left( h^t - BOT - \frac{\Delta z}{2} S_F^t \right). \end{aligned} \quad (6-3)$$

## 6–2 MODFLOW 6 – Supplemental Technical Information

### Standard Formulation

Following the same process used to arrive at equation 5–19 in the [Storage Package Modifications chapter](#), equation 6–3 leads to the following additions to the left- and right-hand sides of the discretized groundwater flow equation:

$$\begin{aligned} A_{n,n} &\leftarrow A_{n,n} - \frac{SC1_n^t}{\Delta t} S_{F_n}^{k-1} \\ b_n &\leftarrow b_n - \frac{SC1_n^{t_{old}}}{\Delta t} S_{F_n}^{t_{old}} \left( h_n^{t_{old}} - BOT_n - \frac{\Delta z_n}{2} S_{F_n}^{t_{old}} \right) + \frac{SC1_n^t}{\Delta t} S_{F_n}^{k-1} \left( BOT_n + \frac{\Delta z_n}{2} S_{F_n}^{k-1} \right). \end{aligned} \quad (6-4)$$

In the absence of specific storage changes, i.e. for  $SC1_n^{t_{old}} = SC1_n^t = SC1_n$ , equation 6–4 simplifies to equation 5–19.

### Newton-Raphson Formulation

Evaluating equation 6–3 cellwise with subscript “*n*” and applying quadratically smoothed cell saturations  $S_F^*$  results in

$$Q_{SS_n} = \frac{SC1_n^{t_{old}}}{\Delta t} S_{F_n}^{*t_{old}} \left( h_n^{t_{old}} - BOT_n - \frac{\Delta z_n}{2} S_{F_n}^{*t_{old}} \right) - \frac{SC1_n^t}{\Delta t} \left[ S_{F_n}^{*t} (h_n^t - BOT_n) + \frac{\Delta z_n}{2} (S_{F_n}^{*t})^2 \right]. \quad (6-5)$$

Upon differentiation of equation 6–5 with respect to  $h_n^t$ , all terms involving  $SC1_n^{t_{old}}$  disappear. The result is equivalent to equation 5–22 with  $SC1_n = SC1_n^t$ :

$$\frac{\partial Q_{SS_n}}{\partial h_n} = -\frac{SC1_n^t}{\Delta t} S_{F_n}^{*t} - \frac{SC1_n^t}{\Delta t} \frac{\partial S_{F_n}^{*t}}{\partial h_n} (h_n^t - BOT_n) + \frac{SC1_n^t}{\Delta t} \Delta z_n S_{F_n}^{*t} \frac{\partial S_{F_n}^{*t}}{\partial h_n}, \quad (6-6)$$

where the superscript “*t*” has been omitted from  $h_n^t$  in the derivatives for clarity. Replacement of  $h_n^t$  and  $S_{F_n}^{*t}$  by their previous iterates,  $h_n^{k-1}$  and  $S_{F_n}^{*k-1}$ , in equations 6–5 and 6–6 and substitution of those equations into equation 5–23 yields the following contributions to  $A_{n,n}$  and  $b_n$ :

$$\begin{aligned} A_{n,n} &\leftarrow A_{n,n} + \left[ -\frac{SC1_n^t}{\Delta t} S_{F_n}^{*k-1} - \frac{SC1_n^t}{\Delta t} \frac{\partial S_{F_n}^{*k-1}}{\partial h_n} (h_n^{k-1} - BOT_n) + \frac{SC1_n^t}{\Delta t} \Delta z_n S_{F_n}^{*k-1} \frac{\partial S_{F_n}^{*k-1}}{\partial h_n} \right] \\ b_n &\leftarrow b_n - \frac{SC1_n^{t_{old}}}{\Delta t} S_{F_n}^{t_{old}} \left( h_n^{t_{old}} - BOT_n - \frac{\Delta z_n}{2} S_{F_n}^{t_{old}} \right) + \frac{SC1_n^t}{\Delta t} S_{F_n}^{*k-1} \left( BOT_n + \frac{\Delta z_n}{2} S_{F_n}^{*k-1} \right) \\ &\quad + \left[ -\frac{SC1_n^t}{\Delta t} \frac{\partial S_{F_n}^{*k-1}}{\partial h_n} (h_n^{k-1} - BOT_n) + \frac{SC1_n^t}{\Delta t} \Delta z_n S_{F_n}^{*k-1} \frac{\partial S_{F_n}^{*k-1}}{\partial h_n} \right] h_n^{k-1}. \end{aligned} \quad (6-7)$$

In the absence of storage changes ( $SC1_n^{t_{old}} = SC1_n^t = SC1_n$ ), equation 6–7 simplifies to equation 5–24.

## Storage Change Integration: Specific Yield

For constant specific yield, MODFLOW 6 calculates the specific yield contribution to groundwater flow ([Langevin and others, 2017](#), eq. 5–10) as

$$Q_{Sy_n} = \frac{SC2_n \Delta z_n}{\Delta t} \left( S_{F_n}^{t_{old}} - S_{F_n}^t \right), \quad (6-8)$$

where  $Q_{Sy_n}$  is the volumetric flow rate from specific yield ( $L^3/T$ ) and  $SC2_n = Sy_n \cdot A_n$  is the secondary storage capacity for cell  $n$  with specific yield  $Sy_n$  and horizontal cell area  $A_n$ .

When specific yield changes transiently, the secondary storage capacity term is expressed in terms of its new value  $SC2_n^t$  and its old value  $SC2_n^{t_{old}}$ , resulting in

$$Q_{Sy_n} = \frac{SC2_n^{t_{old}} \Delta z_n}{\Delta t} S_{F_n}^{t_{old}} - \frac{SC2_n^t \Delta z_n}{\Delta t} S_{F_n}^t. \quad (6-9)$$

## Standard Formulation

Rearranging equation 6–9 for solution at the current iteration  $k$  in terms of  $h_n^k$  instead of saturation  $S_{F_n}^t$  gives

$$Q_{Sy_n}^k = \frac{SC2_n^{t_{old}} \Delta z_n}{\Delta t} S_{F_n}^{t_{old}} - \frac{SC2_n^t \Delta z_n}{\Delta t} \frac{h_n^k - BOT_n}{\Delta z_n}, \quad (6-10)$$

which results in the following contributions to  $A_{n,n}$  and  $b_n$ :

$$\begin{aligned} A_{n,n} &\leftarrow A_{n,n} - \frac{SC2_n^t}{\Delta t} \\ b_n &\leftarrow b_n - \frac{SC2_n^{t_{old}}}{\Delta t} \Delta z_n S_{F_n}^{t_{old}} - \frac{SC2_n^t}{\Delta t} BOT_n. \end{aligned} \quad (6-11)$$

As in the base formulation ([Langevin and others, 2017](#), Chapter 5), for cells where the head at the end of the time step is at or above the top of the cell,  $S_{F_n}^t = 1$  and the specific yield contribution is known. In these cases, no terms are added to  $A_{n,n}$  and the right-hand side contribution instead becomes

$$b_n \leftarrow b_n - \frac{SC2_n^{t_{old}}}{\Delta t} \Delta z_n S_{F_n}^{t_{old}} + \frac{SC2_n^t}{\Delta t} \Delta z_n. \quad (6-12)$$

## Newton-Raphson Formulation

As all  $SC2_n^{t_{old}}$  terms are eliminated by differentiation, the derivative of equation 6–9 at iteration  $k$ , and with quadratically smoothed cell saturations  $S_F^*$  applied, is equivalent to that of the base formulation ([Langevin and others, 2017](#), eq. 5–14) with  $SC2_n = SC2_n^t$ :

$$\frac{\partial Q_{Sy_n}}{\partial h_n} = - \frac{SC2_n^t \Delta z_n}{\Delta t} \frac{\partial S_{F_n}^{*k-1}}{\partial h_n}. \quad (6-13)$$

## 6-4 MODFLOW 6 – Supplemental Technical Information

The fully implicit Newton-Raphson formulation for specific yield storage contribution in cell  $n$  is

$$\frac{\partial Q_{Sy_n}}{\partial h_n} h_n^k = -Q_{Sy_n}^k + \frac{\partial Q_{Sy_n}}{\partial h_n} h_n^{k-1}. \quad (6-14)$$

Substitution of equations 6-9 and 6-13 into equation 6-14 results in the following general expression of the Newton-Raphson formulation for the contribution of specific yield storage to cell  $n$ :

$$\begin{aligned} \left[ -\frac{SC2_n^t \Delta z_n}{\Delta t} \frac{\partial S_{F_n}^{*k-1}}{\partial h_n} \right] h_n^k &= - \left[ \frac{SC2_n^{t_{old}} \Delta z_n}{\Delta t} S_{F_n}^{*t_{old}} - \frac{SC2_n^t \Delta z_n}{\Delta t} S_{F_n}^{*k-1} \right] \\ &\quad + \left[ -\frac{SC2_n^t \Delta z_n}{\Delta t} \frac{\partial S_{F_n}^{*k-1}}{\partial h_n} \right] h_n^{k-1}, \end{aligned} \quad (6-15)$$

which yields the following contributions to  $A_{n,n}$  and  $b_n$ :

$$\begin{aligned} A_{n,n} &\leftarrow A_{n,n} - \frac{SC2_n^t \Delta z_n}{\Delta t} \frac{\partial S_{F_n}^{*k-1}}{\partial h_n} \\ b_n &\leftarrow b_n - \frac{SC2_n^{t_{old}} \Delta z_n}{\Delta t} S_{F_n}^{*t_{old}} + \frac{SC2_n^t \Delta z_n}{\Delta t} S_{F_n}^{*k-1} - \frac{SC2_n^t \Delta z_n}{\Delta t} \frac{\partial S_{F_n}^{*k-1}}{\partial h_n} h_n^{k-1}. \end{aligned} \quad (6-16)$$

For cells where the head at the end of the time step is at or above the top of the cell, the derivative is zero. In these cases, no terms are added to  $A_{n,n}$  and the right-hand side contribution reverts to the standard formulation in equation 6-12.

## Chapter 7. Generalized Coupling of Numerical Models

The multi-model concept was introduced in MODFLOW 6 using GWF Model Exchange objects to support a tight coupling between any two groundwater flow models at the matrix level. This concept has proven to be successful and valued by the modeling community, but the implementation has had its drawbacks too. The information on the spatial discretization at the interface between models as it is available in the Model Exchange object is limited, designed to carry out the basic conductance calculation between connected cells but not sufficient for more advanced discretization schemes. For example, the XT3D option in the NPF package enables simulation of fully three-dimensional (3D) anisotropy by taking into account the full, three-dimensional conductivity tensor [Provost and others \(2017\)](#). In doing so, it requires data not only from any pair of cells between which a flow needs to be calculated but also from their neighboring cells. These data are not available in the Model Exchange object and the XT3D option could not be applied across the model interface, at least not without a significant restructuring of the code.

The extension of MODFLOW 6 with the transport model (GWT) comes with the need for a more generic coupling of sub-models too. Here the XT3D option is used in a similar fashion for the dispersion calculation, and the TVD (total variation diminishing) scheme in the advective transport calculation has a computational stencil (i.e. the group of cells required to determine the flux through a particular cell face) that requires information from neighboring cells as well. Finally, the GWF Model Exchange object merely replicates logic already present in the standard GWF packages, e.g. the standard NPF conductance calculation, the Newton-Raphson formulation, or the cell rewetting algorithm, and is not easily adapted when additions or modifications to those packages are made. We introduce a generalized method for coupling of Numerical Models that addresses these challenges and extends MODFLOW 6 with the capability to couple GWT models.

The generalized coupling uses the concept of an Interface Model and is described in more detail below. In essence, this Interface Model uses the object-oriented paradigm in MODFLOW 6 to mimic a regular GWF or GWT model by means of type extension. This way it can use the existing packages and their algorithms in those models to calculate coefficients for the matrix and right-hand-side vector in the Numerical Solution, a responsibility it takes over from the Model Exchange object on which it relies. Its grid is constructed around the interface defined by the Model Exchange with a sufficiently large extent to perform the calculations. Note that the Interface Model is never being solved and neither its configuration data nor its solution vector have any independent meaning: they are merely an image of those parts of the actual Numerical Models that contribute to the interface grid. As a matter of fact, and this is probably the most important point to make here, this generalized coupling with the Interface Model does not introduce any new model functionality. It even avoids the need for the alternative formulations currently present in the GWF Model Exchange. However, it does enable the user to apply the well-tested concepts of existing MODFLOW 6 packages not only on a model's interior domain, but also across the interface between connected models.

### The Interface Model

Generalized coupling is based on the Interface Model to provide the coefficients for the linear system in Numerical Solution. In order to utilize the routines in the existing flow and transport packages to calculate these coefficients, the grid for the Interface Model is constructed from the individual model grids and the coupling information specified by the user and its package data is kept synchronized with the model data during each step of the simulation. Because the Model Exchange makes it possible to connect model grids of different type (DIS, DISV, and DISU), the resulting interface grid is always unstructured, i.e. of type DISU.

Connecting models such that the dynamics at the interface can be described properly by an Interface Model does impose a few conditions on the configuration. For more advanced functionality such as XT3D, it is required that the relative position of the model grids is specified. They should also share the cell faces over which they are connected, such that the resulting grid for the interface can be specified as a valid DISU dis-

## 7–2 MODFLOW 6 – Supplemental Technical Information

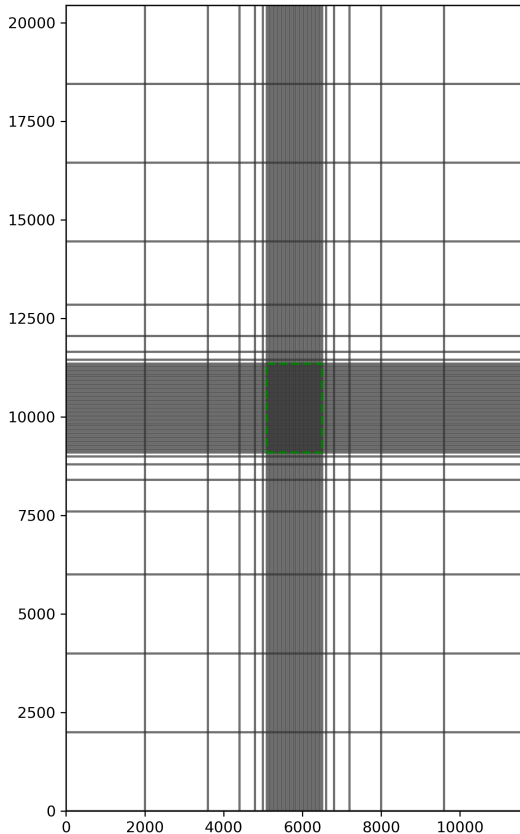


**Figure 7–1.** A plan view of the model grid for the simulation as defined in MT3DMS problem 10. The green dashed rectangle shows the location of the interface that is used for decomposing this case into a system of coupled GWF and GWT models.

cretization. Another consequence is that a certain compatibility is required with respect to the active processes and configuration in the individual models: enabling advection (ADV) or dispersion (DSP), for example, only in one of two connected models introduces ambiguity in how to construct the Interface Model for the transport process. Similar arguments hold when two groundwater models are connected and only one of them is configured with a buoyancy package (BUY). Such model setups are currently not supported.

To illustrate the concept of this new coupling, a well known, single-model case study (problem 10 in the MT3DMS manual [Zheng and Wang \(1999\)](#)) is implemented as a coupled system where the connection between the GWT models is handled by the Interface Model framework. This study is part of the official set of examples that comes with every MODFLOW 6 software release<sup>1</sup>. The coefficients for the flow coupling in this case are calculated with the basic GWF Model Exchange module and the following discussion will focus on the GWT-GWT exchange. Figure 7–1 shows a plan view of the grid and the location of the interface between the submodels. Note that changing only the composition of the grid and leaving the model configuration the same, does not affect the outcome of the simulation<sup>2</sup> and therefore makes for a very suitable test case of this coupling.

Figure 7–2 shows a plan view of the grid that is reconstructed as part of the Interface Model for the inner GWT model. The red band with cells belong to the inner model's grid and the blue cells are part of the outer, coarser grid. Because two Interface Models are constructed for every Exchange, (one for each of the models

<sup>1</sup><https://modflow6-examples.readthedocs.io/en/master/>

<sup>2</sup>At the highest level of detail, the outcome does change because the numbering of the grid nodes is different in both scenarios leading to a reordered matrix system to be solved. As expected, these differences turn out to be well within the configured (IMS) solver tolerance.

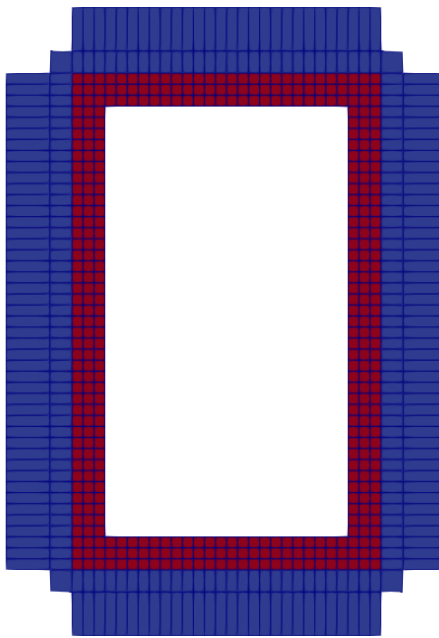


**Figure 7–2.** A top view of the grid for the Interface Model belonging to the inner GWT model in the example described in the text. The blue cells are located in the outer model’s grid, the red cells are internal. Note that deeper layers have an identical horizontal structure..

in it) a similar though not identical picture can be drawn for the outer GWT model. However, the extent of this grid is not necessarily equal on both sides of the exchange. The task of the Interface Model is twofold. First of all, it is designed to calculate the coefficients for the linear system for fluxes through the faces directly at the interface. Additionally, it can provide coefficients for those fluxes that would be affected by cells on the other side of the interface just as if the simulation would have been set up as a single model. It is the requirement to support the latter that causes the asymmetry. This becomes clearer when looking at Figure 7–3 which shows the XT3D computational stencils and how they determine what the required extent of the interface grid is. To determine the flux through a face at the model interface, the cells on either side and their immediate neighbors are sufficient (the circle). To correctly calculate the flux through cell faces not directly at the interface but influenced by the connection to another model, more additional levels of connectivity are required, depending on the exact size of the computation stencil (the diamond).

This case study is used to demonstrate the concept of the generalized coupling method with the Interface Model. It serves as an excellent test case because the outcome should be identical to the known results, at least within the configured tolerance of the Numerical Solution. However, from a modeling perspective it would make more sense to redesign the model grid of the problem. With the new capability to use the multi-model approach also for problems containing solute transport, there is no longer a need to refine the study area by using varying column and row width as was done in the original MT3DMS problem. Both the study area and the surrounding domain can be configured as coupled models with a regularly structured (DIS) grid. The granularity of the inner grid can be independently refined to improve the resolution of the results without the need to set up the entire problem based on an unstructured (DISU) grid.

## 7–4 MODFLOW 6 – Supplemental Technical Information

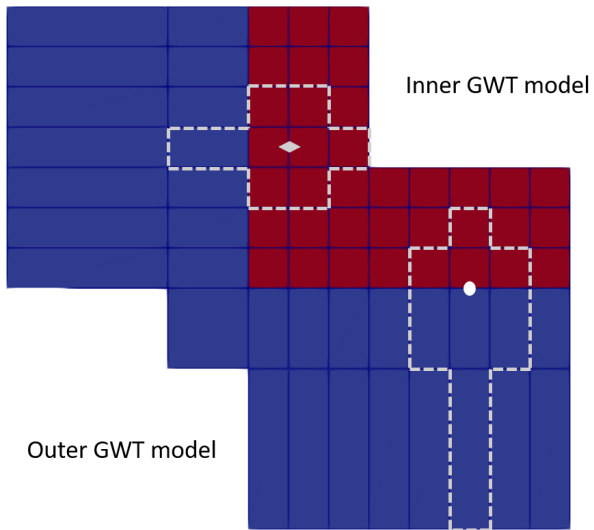


**Figure 7–3.** Top view when zoomed in to the South-West corner of the interface grid. The dashed line surrounds the grid cells participating in the calculation of the dispersive XT3D flux directly at the interface (the white circle) and through a face in the model's interior (the white diamond) which is nonetheless affected by the connection to the outer GWT model. The extension of the computational stencil in the vertical direction is omitted but straightforward..

Finally, such a setup would allow to apply the Interface Model in another powerful way. A refinement of the grid is known to produce inaccuracies at the interface, as discussed in the introduction of [Provost and others \(2017\)](#). This can be remedied by enabling the XT3D option in the GWF NPF package. The new coupling mechanism based on the Interface Model makes it now possible to enable this option *only* at the interface, which will mitigate the distorting effects of such a grid refinement on the calculated flow field and still avoids the computational overhead of calculating the XT3D terms on the entire domain.

## Chapter 8. Accounting for Fluid Viscosity

The dynamic viscosity of a fluid is a function of fluid composition and temperature and typically has a weak dependence on pressure. In some applications, particularly those that involve large variations in temperature, viscosity can vary significantly in space and over time. Variations in viscosity, in turn, can affect groundwater flow by changing the hydraulic conductivity, which is inversely proportional to viscosity. In the original release of MODFLOW 6, variations in viscosity and their effects on hydraulic conductivity were not taken into account. The MODFLOW 6 Viscosity (VSC) Package allows viscosity to vary as a function of solute concentrations and fluid temperature and accounts for the effect of variable viscosity on hydraulic conductivity in the Node-Property Flow (NPF) Package and in stress packages that involve head-dependent groundwater flow. Temperature-dependent viscosity has been implemented in other groundwater modeling codes, including HST3D (Kipp, 1987), VS2DH (Healy and Ronan, 1996), SUTRA-MS (Hughes and Sanford, 2004), and SEAWAT Version 4 (Langevin and others, 2008). Like these other codes, the VSC Package does not account for the dependence of viscosity on pressure, which is negligible in most applications.

For cases in which the rate of groundwater flow is proportional to the head gradient in the direction of flow, as in an isotropic porous medium, the flow between two adjacent locations can be approximated using a one-dimensional form of Darcy's Law (Langevin and others, 2017, equation 4-15):

$$Q = C (h_1 - h_2), \quad (8-1)$$

where  $h_1$  and  $h_2$  are the hydraulic heads at locations 1 and 2, respectively,  $Q$  is the flow from location 1 to location 2, and  $C$  is a hydraulic conductance defined by (Langevin and others, 2017, equation 4-14):

$$C = \frac{KA}{L_{1,2}}, \quad (8-2)$$

where  $K$  is the hydraulic conductivity of the porous medium that connects the two locations,  $A$  is the cross-sectional area perpendicular to flow, and  $L_{1,2}$  is the distance between two locations. A form of equation 8-1 is used in the MODFLOW 6 "conductance-based" formulation for flow between two adjacent model cells (Langevin and others, 2017). In that case, the conductance is based on an effective hydraulic conductivity between the two cells, the area of the cell-cell interface, and the distance between the cell centers. A form of equation 8-1 is also used in MODFLOW 6 stress packages in which the flow into or out of the model at a model boundary is head-dependent. For example, in the General-Head Boundary (GHB) Package, flow between an external source and a groundwater model cell is proportional to the difference between the head assigned to the external source and the simulated head in the cell, and the conductance is representative of the material between the external source and the cell center.

Because hydraulic conductivity is inversely proportional to viscosity, the conductivity  $K$  for a simulated fluid composition and temperature is related to the conductivity  $K_0$  for some reference composition and temperature by

$$K = \frac{\mu_0}{\mu} K_0. \quad (8-3)$$

It follows from equation 8-2 that the conductance  $C$  for a simulated fluid composition and temperature is related to the conductance  $C_0$  for the reference composition and temperature by

## 8–2 MODFLOW 6 – Supplemental Technical Information

$$C = \frac{\mu_0}{\mu} C_0, \quad (8-4)$$

where  $\mu$  and  $\mu_0$  are the viscosities at the simulated and reference conditions, respectively. The VSC Package uses equations 8–3 and 8–4 to update hydraulic conductivities and conductances to account for changes in solute concentrations and temperature during a flow and transport simulation based on the Groundwater Flow (GWF) and Groundwater Transport (GWT) Models. The GWT Model is designed to simulate solute transport but can be used to simulate heat transport in some applications by appropriately scaling the input parameters to render the solute-transport equation mathematically equivalent to the heat-transport equation (Zheng, 2010). In such cases, the “solute concentration” calculated by a GWT-based heat-transport model can be identified in the VSC Package input file as representing temperature. Although the VSC Package allows viscosity to vary with solute concentration, variations in viscosity are typically most significant in heat-transport applications.

### Dependence of Viscosity on Concentration and Temperature

The VSC Package calculates viscosity as a function of concentration and temperature using the following equation (Langevin and others, 2008, equation 17):

$$\mu = \mu_T(T) + \sum_{k=1}^{NS} \frac{\partial \mu}{\partial C^k} (C^k - C_0^k) \quad (8-5)$$

where  $NS$  is the number of chemical species (solutes) whose concentrations affect viscosity,  $C^k$  and  $C_0^k$  are the simulated and user-specified reference concentrations of species  $k$ , respectively, and  $\partial \mu / \partial C^k$  is the user-specified rate at which viscosity changes linearly with the concentration of species  $k$ . (Symbols  $C^k$  and  $C_0^k$  are not to be confused with the symbols for conductance,  $C$  and  $C_0$ , introduced earlier.) When all concentrations are equal to their reference values, the viscosity is equal to  $\mu_T(T)$ , which embodies the dependence of viscosity on temperature according to

$$\mu_T(T) = \begin{cases} \mu_0 + \frac{\partial \mu}{\partial T} (T - T_0) & \text{linear} \\ \mu_0 A_2^{\frac{A_3(T_0-T)}{(T+A_4)(T_0+A_4)}} & \text{nonlinear} \end{cases}. \quad (8-6)$$

where  $T$  and  $T_0$  are the simulated and user-specified reference temperature, respectively, and  $\mu_0$  is the user-specified reference viscosity. The reference viscosity is commonly set to  $0.001 \text{ kg m}^{-1} \text{ s}^{-1}$ , which is representative of freshwater at a reference temperature of  $20^\circ\text{C}$  (Maidment, 1993, Table 11.1). When  $T$  equals  $T_0$ , or if temperature is not designated by the user as affecting viscosity,  $\mu_T(T)$  equals  $\mu_0$ . Equation 8–6 includes both linear and nonlinear variation of viscosity with temperature. Linear variation is the default, in which case  $\partial \mu / \partial T$  is the user-specified rate at which viscosity changes linearly with temperature. Nonlinear variation is a user-selectable option, in which case the variation of viscosity from the reference value is determined by user-specified parameters  $A_2$ ,  $A_3$ , and  $A_4$ . The nonlinear option in equation 8–6 is mathematically equivalent to one of the options available in SEAWAT Version 4 (Guo and Langevin, 2002, equation 18) but is written in a form that explicitly sets  $\mu_T(T)$  equal to  $\mu_0$  when  $T$  equals  $T_0$ . Setting  $\mu_0$ ,  $A_2$ ,  $A_3$ , and  $A_4$  to  $0.001002 \text{ kg m}^{-1} \text{ s}^{-1}$ ,  $10.0$ ,  $248.37$ , and  $133.15$ , respectively, and rounding the lead coefficient to one decimal place gives the temperature dependence of viscosity used in SUTRA (Voss, 1984) and SUTRA-MS (Hughes and

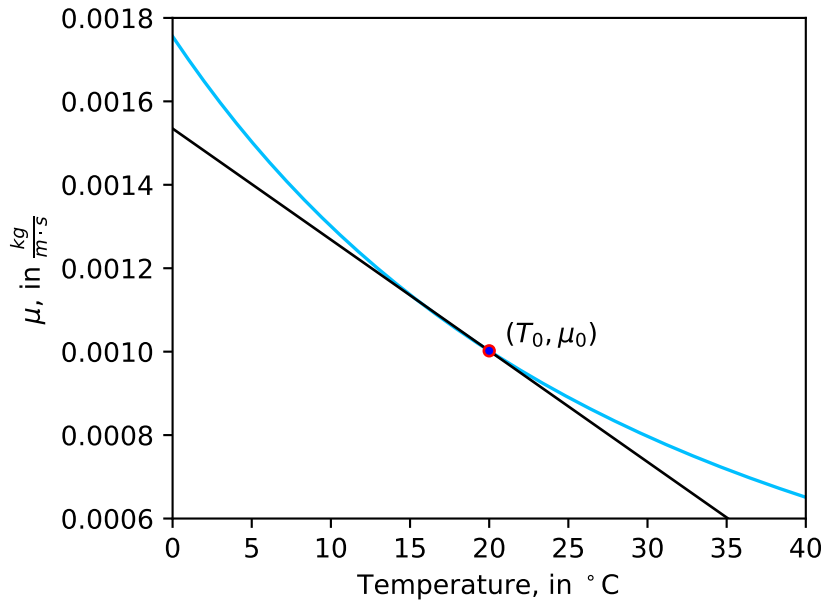


**Figure 8-1.** Nonlinear dependence of viscosity on temperature (blue curve) that is representative of freshwater over the temperature range 0 – 40°C, and a linear approximation (black curve) that has the same value ( $\mu_0$ ) and slope at the reference temperature ( $T_0$ ). The blue curve is generated using 0.001002 kg m<sup>-1</sup> s<sup>-1</sup>, 10.0, 248.37, and 133.15 for  $\mu_0$ ,  $A_2$ ,  $A_3$ , and  $A_4$ , respectively.

Sanford, 2004). VS2DH (Healy and Ronan, 1996) also calculate the temperature dependence of viscosity using functions that are, respectively, mathematically equivalent to and a special case of equation 8-6.

Over the temperature range 0 – 40°C, the viscosity of freshwater varies between approximately 0.0007 and 0.00175 kg m<sup>-1</sup> s<sup>-1</sup>, as indicated by the nonlinear (blue) curve in figure 8-1. The black line in figure 8-1 depicts a linear approximation that coincides with the nonlinear curve at the reference temperature and viscosity,  $(T_0, \mu_0) = (20^\circ\text{C}, 0.001 \text{ kg m}^{-1} \text{ s}^{-1})$ .

## Accounting for Variable Viscosity in Flows Between Cells

The VSC Package uses concentrations and temperatures calculated for each cell by a GWT model on the previous time step or outer solution iteration to calculate viscosities for the current time step. These viscosities are used to adjust cell hydraulic conductivity values in the NPF Package using equation 8-3. The reference values of conductivity are the values specified by the user in the NPF Package and, optionally, the Time-Varying Conductivity (TVK) Package (Chapter 6 of this document). The conductivity adjustment is performed after the user-specified conductivities are read in but before conductivity values are passed to program units that use cell conductivities to formulate expressions for flow between cells, which include the “conductance-based” formulation for flow and the XT3D capability (Provost and others, 2017). If the VSC Package is not active, cell conductivities are not adjusted for variable viscosity, and the user-specified values are used.

## Accounting for Variable Viscosity in Boundary Flows

The VSC Package uses concentrations and temperatures calculated for each cell by a GWT model on the previous time step or outer solution iteration in calculating viscosities for the current time step. These viscosities are used to adjust hydraulic conductances, using equation 8-4, in stress packages that involve head-

## **8–4 MODFLOW 6 – Supplemental Technical Information**

dependent boundary flows, which include the River (RIV), General-Head Boundary (GHB), Drain (DRN), Streamflow Routing (SFR), Lake (LAK), and Multi-Aquifer Well (MAW) Packages ([Langevin and others, 2017](#)). For a boundary flow out of the model, the viscosity is based on the simulated concentration or temperature in the cell from which the boundary flow originates. For a boundary flow into the model, the viscosity is based on the concentration or temperature of the water entering the cell from the boundary. The reference values of conductance are the values normally set or calculated by the stress package based on user input. The conductance adjustment is performed after the stress package completes its normal conductance calculation but before the conductance value is used to formulate the expression for the boundary flow. If the VSC Package is not active, stress-package conductances are not adjusted for variable viscosity.

## Chapter 9. Revised Parameterization of Transport for Combined Mobile and Immobile Domain Simulations

The Groundwater Transport (GWT) Model ([Langevin and others, 2022](#)) in MODFLOW 6 can simulate a variety of solute-transport processes in aquifer material that includes “mobile” and “immobile” domains. The mobile and immobile domains are conceptualized as coexisting within a model cell and can exchange solute with each other. The mobile domain is always simulated by the GWT Model. Transport in an immobile domain, which may be optionally defined by the user, is simulated by the Immobile Storage and Transfer (IST) Package ([Langevin and others, 2022](#)) for the GWT Model. Multiple instances of the IST Package may be invoked to represent multiple immobile domains.

In MODFLOW 6 version 6.4.2, the parameterization of the equations that govern transport in the mobile and immobile domains has been revised, and corresponding changes have been made to the input requirements for porosity, domain fraction, and bulk density. The revised parameterization is expected to be more intuitive for users in many mobile-immobile transport applications. It will also allow users to model a wider variety of solute transport scenarios involving immobile-domain sorption than the original parameterization used in versions of MODFLOW 6 up to and including version 6.4.1.

Input for existing MODFLOW 6 models that include one or more immobile domains can be converted from the original parameterization to the revised parameterization such that the simulated transport behavior remains the same. No changes to the model input are needed for existing MODFLOW 6 models that do not include an immobile domain.

The remainder of this chapter begins with a review of the original parameterization of transport described in ([Langevin and others, 2022](#)). The revised parameterization is then presented, and guidance is provided for converting existing model input from the original parameterization to the revised parameterization.

### Review of the Original Parameterization

With the original parameterization used in versions of MODFLOW 6 up to and including version 6.4.1, the partial differential equation that represents the conservation of solute mass at points in the mobile domain is equation 2–1 of [Langevin and others \(2022\)](#), which is reproduced here as

$$\frac{\partial (S_w \theta_m C)}{\partial t} = -\nabla \cdot (\mathbf{q}C) + \nabla \cdot (S_w \theta_m \mathbf{D} \nabla C) + q'_s C_s + M_s - \lambda_1 \theta_m S_w C - \gamma_1 \theta_m S_w \\ - f_m \rho_b \frac{\partial (S_w \bar{C})}{\partial t} - \lambda_2 f_m \rho_b S_w \bar{C} - \gamma_2 f_m \rho_b S_w - \sum_{im=1}^{nim} \zeta_{im} S_w (C - C_{im}) \quad (9-1)$$

where  $S_w$  is the water saturation defined as the volume of water per volume of voids ( $L^3/L^3$ ),  $C$  is the mobile-domain volumetric concentration of solute expressed as mass of dissolved solute per unit volume of mobile-domain fluid ( $M/L^3$ ),  $t$  is time ( $T$ ),  $\mathbf{q}$  is the vector of specific discharge ( $L/T$ ),  $\mathbf{D}$  is the second-order tensor of hydrodynamic dispersion coefficients ( $L^2/T$ ),  $q'_s$  is the volumetric flow rate per unit volume of aquifer (defined as positive for flow into the aquifer) for mass sources and sinks ( $1/T$ ),  $C_s$  is the volumetric solute concentration of the source or sink fluid ( $M/L^3$ ),  $M_s$  is rate of solute mass loading per unit volume of aquifer ( $M/L^3T$ ),  $\lambda_1$  is the first-order decay rate coefficient for dissolved solute in the mobile domain ( $1/T$ ),  $\gamma_1$  is the zero-order decay rate coefficient for dissolved solute in the mobile domain ( $M/L^3T$ ),  $\bar{C}$  is the mass-fraction concentration of sorbate (sorbed solute) expressed as mass of sorbate per unit mass of solid aquifer material in the mobile domain ( $M/M$ ),  $\lambda_2$  is the first-order decay rate coefficient ( $1/T$ ) for sorbate in the mobile domain,  $\gamma_2$  is the zero-order decay rate coefficient ( $M/MT$ ) for sorbate in the mobile domain,  $nim$  is the number of immobile domains,  $\zeta_{im}$  is the rate coefficient for the transfer of mass between the mobile domain

## 9–2 MODFLOW 6 – Supplemental Technical Information

and immobile domain  $im$  ( $1/T$ ),  $C_{im}$  is an immobile-domain volumetric concentration of solute expressed as mass of dissolved solute per unit volume of fluid in immobile domain  $im$  ( $M/L^3$ ),  $\rho_b$  is the bulk density of the aquifer material defined as the mass of solid aquifer material per unit volume of aquifer ( $M/L^3$ ),  $\theta_m$  is the mobile-domain effective porosity defined as volume of voids participating in mobile-domain transport per unit volume of aquifer ( $L^3/L^3$ ), and  $f_m$  is the fraction of the mass of aquifer solid material that is in the mobile domain ( $M/M$ ). To avoid potential confusion with the total porosity, in equation 9–1 the mobile porosity is intentionally given the symbol  $\theta_m$ , which is different than the symbol  $\theta$  used by [Langevin and others \(2022\)](#). Also, note that [Langevin and others \(2022\)](#) define  $f_m$  as “the fraction of aquifer solid material available for sorptive exchange with the mobile phase under fully saturated conditions,” which is correct only if all the aquifer solid material in the mobile domain is available for sorptive exchange and the fraction is understood to be a mass fraction.

The Immobile Storage and Transfer (IST) Package for the GWT Model allows users to designate a fraction of a model cell as immobile. With the original parameterization used in versions of MODFLOW 6 up to and including version 6.4.1, the partial differential equation that represents the conservation of solute mass at points in an immobile domain is equation 7–2 of [Langevin and others \(2022\)](#), which is reproduced here as

$$\theta_{im} \frac{\partial C_{im}}{\partial t} + f_{im} \rho_b \frac{\partial \bar{C}_{im}}{\partial t} = -\lambda_{1,im} \theta_{im} C_{im} - \lambda_{2,im} f_{im} \rho_b \bar{C}_{im} \\ -\gamma_{1,im} \theta_{im} - \gamma_{2,im} f_{im} \rho_b + \zeta_{im} S_w (C - C_{im}), \quad (9-2)$$

where  $\bar{C}_{im}$  is the mass-fraction concentration of sorbate (sorbed solute) expressed as mass of sorbate per unit mass of solid aquifer material in the immobile domain ( $M/M$ ),  $\lambda_{1,im}$  is the first-order reaction rate coefficient for dissolved solute in the immobile domain ( $1/T$ ),  $\lambda_{2,im}$  is the first-order reaction rate coefficient for sorbate in the immobile domain ( $1/T$ ),  $\gamma_{1,im}$  is the zero-order reaction rate coefficient for dissolved solute in the immobile domain ( $ML^{-3}T^{-1}$ ),  $\gamma_{2,im}$  is the zero-order reaction rate coefficient for sorbate in the immobile domain ( $MM^{-1}T^{-1}$ ),  $\theta_{im}$  is the effective porosity in the immobile domain defined as volume of voids participating in immobile-domain transport per unit volume of immobile domain  $im$  ( $L^3/L^3$ ), and  $f_{im}$  is the fraction of the mass of aquifer solid material that is in immobile domain  $im$  ( $M/M$ ). Note that [Langevin and others \(2022\)](#) define  $f_{im}$  as “the fraction of aquifer solid material available for sorptive exchange with the immobile domain under fully saturated conditions,” which is correct only if all the aquifer solid material in the immobile domain is available for sorptive exchange and the fraction is understood to be a mass fraction.

The original model parameters that are affected by the revised parameterization are listed in table 9–1. Note that in the original parameterization, division of the aquifer into mobile and immobile domains is conceptualized in terms solid mass fractions, and porosities and bulk densities are defined on a per-aquifer-volume basis. Note also that the user is required (in versions of MODFLOW 6 up to and including version 6.4.1) to provide the value of the overall bulk density,  $\rho_b$ , in the input for each package that represents a domain in which sorption is active (the MST Package for the mobile domain, and the IST Package for immobile domains).

Immobile-domain solid mass fractions,  $f_{im}$ , are not input by the user; rather, they are calculated by MODFLOW 6 (in versions up to and including 6.4.1) from user-input porosities using

$$f_{im} = \frac{\theta_{im}}{\theta_t}. \quad (9-3)$$

where  $\theta_t$  is the total porosity [which is erroneously represented by the symbol  $\theta$  in the related text on p. 7–2 of [Langevin and others \(2022\)](#)]. The mobile-domain solid mass fraction is then calculated by MODFLOW 6 (in versions up to and including 6.4.1) using

**Table 9–1.** Symbols, descriptions, and definitions of original mobile and immobile domain model parameters (used in versions of MODFLOW 6 up to and including version 6.4.1) that are affected by the revised parameterization. In the original parameterization, division of the aquifer into domains is conceptualized in terms of solid mass fractions, and domain properties are defined on a per-aquifer-volume basis.

Symbol	Description	Definition	Notes
$\theta_m$	porosity (mobile domain)	$\frac{\text{mobile domain pore volume}}{\text{aquifer volume}}$	sorption-related input parameter
$\theta_{im}$	porosity (immobile domain $im$ )	$\frac{\text{immobile domain pore volume}}{\text{aquifer volume}}$	sorption-related input parameter
$\rho_b$	overall bulk density (mobile and immobile domains combined)	$\frac{\text{aquifer solid mass}}{\text{aquifer volume}}$	sorption-related input parameter
$f_m$	solid mass fraction (mobile domain)	$\frac{\text{mobile domain solid mass}}{\text{aquifer solid mass}}$	sorption-related parameter (not input; calculated by MODFLOW 6 from immobile-domain solid mass fractions)
$f_{im}$	solid mass fraction (immobile domain $im$ )	$\frac{\text{immobile domain solid mass}}{\text{aquifer solid mass}}$	sorption-related parameter (not input; calculated by MODFLOW 6 from user-specified domain porosities)

$$f_m = 1 - \sum_{im} f_{im}, \quad (9-4)$$

where the summation is over all immobile domains specified by the user. Equations 9–4 and 9–3, together with the definition of total porosity,

$$\theta_t = \theta_m + \sum_{im} \theta_{im}, \quad (9-5)$$

imply that the default value of the mobile domain solid mass fraction is given by

$$f_m = 1 - \sum_{im} f_{im} = 1 - \frac{\sum_{im} \theta_{im}}{\theta_t} = \frac{\theta_m}{\theta_t}. \quad (9-6)$$

If there are no immobile domains, the total porosity is the same as the mobile porosity and  $f_m$  is 1.

## Revised Parameterization

The revised parameterization described in this chapter differs from the original parameterization, which is described in [Langevin and others \(2022\)](#) and summarized above, in the following ways:

## 9–4 MODFLOW 6 – Supplemental Technical Information

- Two sets of parameter substitutions are implemented in governing equations 9–1 and 9–2. These substitutions recast the model input in terms of parameters that are expected to be more intuitive for users in many applications.
  - Domain porosities  $\theta_m$  and  $\theta_{im}$ , which are defined on a per-aquifer-volume basis, are replaced by the mathematically equivalent expressions  $\hat{f}_m\phi_m$  and  $\hat{f}_{im}\phi_{im}$ , respectively, where  $\hat{f}_m$  and  $\hat{f}_{im}$  are domain volume fractions (instead of mass fractions) and  $\phi_m$  and  $\phi_{im}$  are domain porosities defined on a per-domain-volume basis.
  - The parameter products  $f_m\rho_b$  and  $f_{im}\rho_b$  are replaced by the mathematically equivalent products  $\hat{f}_m\rho_{b,m}$  and  $\hat{f}_{im}\rho_{b,im}$ , respectively, where  $\rho_{b,m}$  and  $\rho_{b,im}$  are domain bulk densities defined on a per-domain-volume basis.
- Unlike the domain mass fractions  $f_m$  and  $f_{im}$ , which are set automatically by MODFLOW 6 (in versions up to and including 6.4.1) based on domain porosities in the original parameterization, the domain volume fractions  $\hat{f}_m$  and  $\hat{f}_{im}$  are specified directly by the user in the revised parameterization, offering the flexibility to accurately characterize sorption in a wider variety of mobile-immobile systems.

With the changes to the parameterization summarized above, the partial differential equations that represent the conservation of solute mass at points in the mobile and immobile domains can be written as

$$\begin{aligned} \frac{\partial (S_w\theta_m C)}{\partial t} = & -\nabla \cdot (\mathbf{q}C) + \nabla \cdot (S_w\theta_m \mathbf{D}\nabla C) + q'_s C_s + M_s - \lambda_1 \theta_m S_w C - \gamma_1 \theta_m S_w \\ & - \hat{f}_m \rho_{b,m} \frac{\partial (S_w \bar{C})}{\partial t} - \lambda_2 \hat{f}_m \rho_{b,m} S_w \bar{C} - \gamma_2 \hat{f}_m \rho_{b,m} S_w - \sum_{im=1}^{nim} \zeta_{im} S_w (C - C_{im}) \end{aligned} \quad (9-7)$$

where

$$\theta_m = \hat{f}_m \phi_m, \quad (9-8)$$

and

$$\begin{aligned} \theta_{im} \frac{\partial C_{im}}{\partial t} + \hat{f}_{im} \rho_{b,im} \frac{\partial \bar{C}_{im}}{\partial t} = & -\lambda_{1,im} \theta_{im} C_{im} - \lambda_{2,im} \hat{f}_{im} \rho_{b,im} \bar{C}_{im} \\ & - \gamma_{1,im} \theta_{im} - \gamma_{2,im} \hat{f}_{im} \rho_{b,im} + \zeta_{im} S_w (C - C_{im}), \end{aligned} \quad (9-9)$$

where

$$\theta_{im} = \hat{f}_{im} \phi_{im}. \quad (9-10)$$

respectively. Model parameters and variables in equations 9–7 and 9–9 are defined as in equations 9–1 and 9–2, except for the new parameters introduced in the revised parameterization:  $\hat{f}_m$  is the volume fraction of the mobile domain defined as the volume of mobile domain per volume of aquifer ( $L^3/L^3$ ),  $\hat{f}_{im}$  is the volume fraction of the immobile domain defined as the volume of mobile domain  $im$  per volume of aquifer ( $L^3/L^3$ ),  $\rho_{b,m}$  is the bulk density of aquifer material in the mobile domain defined as mass of solid aquifer material per unit volume of mobile domain ( $M/L^3$ ),  $\rho_{b,im}$  is the bulk density of aquifer material in the immobile domain

defined as mass of solid aquifer material per unit volume of immobile domain  $im$  ( $M/L^3$ ),  $\phi_m$  is the mobile-domain effective porosity defined as volume of voids participating in mobile-domain transport per unit volume of mobile domain ( $L^3/L^3$ ), and  $\phi_{im}$  is the effective porosity in the immobile domain defined as defined as volume of voids participating in immobile-domain transport per unit volume of mobile domain  $im$  ( $L^3/L^3$ ). In the MODFLOW 6 code, porosities  $\theta_m$  and  $\theta_{im}$  are calculated from the new input parameters using equations 9–8 and 9–10 before being incorporated into discretized representations of equations 9–7 and 9–9. The new parameters are discussed in more detail below.

## Revised Parameters

The new parameters are summarized in table 9–2. Note that in the revised parameterization, division of the aquifer into mobile and immobile domains is conceptualized in terms of volume fractions, and porosities and bulk densities are defined on a per-domain-volume basis. When an aquifer can be divided into multiple domains that occupy distinct, well-defined volumes, as when the mobile and immobile domains represent different lithologies, it may be intuitive to think in terms of the domain volume fractions and local domain properties (properties defined on a per-domain-volume basis).

**Table 9–2.** Symbols, descriptions, and definitions of revised mobile and immobile domain model parameters introduced in MODFLOW 6 version 6.4.2. In the revised parameterization, division of the aquifer into domains is conceptualized in terms of volume fractions, and domain properties are defined on a per-domain-volume basis.

Symbol	Description	Definition	Notes
$\phi_m$	porosity (mobile domain)	$\frac{\text{mobile domain pore volume}}{\text{mobile domain volume}}$	transport input parameter (not directly related to sorption)
$\phi_{im}$	porosity (immobile domain $im$ )	$\frac{\text{immobile domain pore volume}}{\text{immobile domain volume}}$	transport input parameter (not directly related to sorption)
$\rho_{b,m}$	bulk density (mobile domain)	$\frac{\text{mobile domain solid mass}}{\text{mobile domain volume}}$	sorption-related input parameter
$\rho_{b,im}$	bulk density (immobile domain $im$ )	$\frac{\text{immobile domain solid mass}}{\text{immobile domain volume}}$	sorption-related input parameter
$\hat{f}_m$	volume fraction (mobile domain)	$\frac{\text{mobile domain volume}}{\text{aquifer volume}}$	transport and sorption-related parameter (not input; calculated by MODFLOW 6 from immobile-domain volume fractions)
$\hat{f}_{im}$	volume fraction (immobile domain $im$ )	$\frac{\text{immobile domain volume}}{\text{aquifer volume}}$	transport and sorption-related input parameter

All parameters in table 9–2 are model input parameters except the mobile-domain volume fraction,  $\hat{f}_m$ , which is calculated by MODFLOW 6 from the user-specified immobile-domain volume fractions using

$$\hat{f}_m = 1 - \sum_{im} \hat{f}_{im}, \quad (9-11)$$

where the summation is over all immobile domains specified by the user. If there are no immobile domains,  $\hat{f}_m$  is set to 1.

## 9–6 MODFLOW 6 – Supplemental Technical Information

Porosities and bulk densities in table 9–2 are defined on a per-domain-volume basis, i.e., as an amount per unit volume of domain. The total porosity,  $\theta_t$ , can be calculated as the volume-weighted average of the domain porosities,  $\phi_m$  and  $\phi_{im}$ :

$$\theta_t = \theta_m + \sum_{im} \theta_{im} = \hat{f}_m \phi_m + \sum_{im} \hat{f}_{im} \phi_{im}, \quad (9-12)$$

Similarly, the overall bulk density,  $\rho_b$ , can be calculated as the volume-weighted average of the domain bulk densities,  $\rho_{b,m}$  and  $\rho_{b,im}$ :

$$\rho_b = \hat{f}_m \rho_{b,m} + \sum_{im} \hat{f}_{im} \rho_{b,im}. \quad (9-13)$$

### Conversion of Existing Model Input to the Revised Parameterization

Conversion of existing MODFLOW 6 model input to the revised parameterization such that the simulation gives the same numerical results requires that the revised mobile-domain solute conservation equation, equation 9–7, be numerically equivalent to the original mobile-domain solute conservation equation, equation 9–1. This is achieved when  $\hat{f}_m$  and  $\phi_m$  satisfy

$$\hat{f}_m \phi_m = \theta_m \quad (9-14)$$

and, if sorption is active in the mobile domain,  $\hat{f}_m$  and  $\rho_{b,m}$  satisfy

$$\hat{f}_m \rho_{b,m} = f_m \rho_b. \quad (9-15)$$

For a model that includes at least one immobile domain, the revised immobile-domain solute conservation equation, equation 9–9, must also be numerically equivalent to the original immobile-domain solute conservation equation, equation 9–2. This is achieved when  $\hat{f}_{im}$  and  $\phi_{im}$  satisfy

$$\hat{f}_{im} \phi_{im} = \theta_{im} \quad (9-16)$$

and, if sorption is active in immobile domain  $im$ ,  $\hat{f}_{im}$  and  $\rho_{b,im}$  satisfy

$$\hat{f}_{im} \rho_{b,im} = f_{im} \rho_b. \quad (9-17)$$

### Simulation Without Immobile Domains

For an existing simulation without immobile domains, which is the most common use case, no conversion of input parameters is needed to obtain the same simulation results. In this case, MODFLOW 6 sets  $f_m = 1$  in the original parameterization and  $\hat{f}_m = 1$  in the revised parameterization. Thus, equations 9–14 and 9–15 reduce to  $\phi_m = \theta_m$  and  $\rho_{b,m} = \rho_b$ , respectively, and are satisfied by default by the original input values.

## Simulation With At Least One Immobile Domain

For an existing simulation that includes at least one immobile domain, the values of the revised input parameters  $\phi_m$ ,  $\phi_{im}$ , and  $\hat{f}_{im}$  must be set such that they satisfy equations 9–14 and 9–16 in order to obtain the same simulation results. The value of  $\hat{f}_m$  is calculated by MODFLOW 6 using equation 9–11. Note that the immobile-domain fractions  $\hat{f}_{im}$  must sum to less than one so that the resulting mobile-domain fraction,  $\hat{f}_m$ , is greater than zero.

If the existing simulation also includes sorption, the value of the domain bulk density ( $\rho_{b,m}$  or  $\rho_{b,im}$ ) must be specified for each domain in which sorption is active. For a mobile domain with sorption,  $\rho_{b,m}$  must satisfy equation 9–15. For an immobile domain with sorption,  $\rho_{b,im}$  must satisfy equation 9–17.

Because the revised parameterization involves more input parameters than the original parameterization, the choice of new parameter values that produce the same simulation results is not unique. One approach, for example, is to specify the values of the immobile domain fractions  $\hat{f}_{im}$ . The required values of  $\hat{f}_m$ ,  $\phi_m$ ,  $\rho_{b,m}$ ,  $\phi_{im}$ , and  $\rho_{b,im}$  are then determined by equations 9–11 and 9–14 – 9–17, respectively. If the only goal is to obtain the same simulation results, without regard for whether the revised parameter values are realistic or representative of the domains being modeled, one may, for example, set each immobile domain fraction to  $\hat{f}_{im} = 1/N_{dom}$ , where  $N_{dom}$  is the total number of domains including the mobile domain.

## Unrealistic Parameter Values

It is possible that in some cases the process of converting parameters will produce revised parameter values that are unrealistic or inconsistent with independently measured or estimated values. For example, selection of apparently reasonable values of  $\hat{f}_{im}$  may require setting  $\hat{f}_m$ ,  $\phi_m$ ,  $\rho_{b,m}$ ,  $\phi_{im}$ , and/or  $\rho_{b,im}$  to unreasonable values. Assuming the conversion equations have been applied correctly and the independently measured or estimated values are reasonably accurate, other possible sources of inconsistency are errors in setting the original parameter values; selection of unrealistic values for revised parameters ( $\hat{f}_{im}$  values, for example) as a starting point for the conversion; and the setting of the original immobile domain fractions  $f_{im}$  according to equation 9–3, which may be a poor approximation for some of the domains being modeled.

## References Cited

- Guo, W., and Langevin, C.D., 2002, User's Guide to SEAWAT: A Computer Program for Simulation of Three-Dimensional Variable-Density Ground-Water Flow: U.S. Geological Survey Techniques of Water-Resources Investigations book 6, Chapter A7, 77 p., accessed July 25, 2019, at <https://pubs.er.usgs.gov/publication/ofr03426>.
- Harbaugh, A.W., 2005, MODFLOW-2005, the U.S. Geological Survey modular ground-water model—the Ground-Water Flow Process: U.S. Geological Survey Techniques and Methods, book 6, chap. A16, variously paged, accessed June 27, 2017, at <https://pubs.usgs.gov/tm/2005/tm6A16/>.
- Healy, R.W., and Ronan, A.D., 1996, Documentation of Computer Program VS2DH for Simulation of Energy Transport in Variably Saturated Porous Media: Modification of the U.S. Geological Survey's Computer Program VS2DT: U.S. Geological Survey Water-Resources Investigation Report 96-4230, 36 p., accessed September 27, 2022, at <https://doi.org/10.3133/wri964230>, at <https://pubs.usgs.gov/wri/1996/4230/report.pdf>.
- Hughes, J.D., and Sanford, W.E., 2004, SUTRA-MS: A version of SUTRA modified to simulate heat and multiple-solute transport: U.S. Geological Survey Open File Report 2004-1207, 141 p., accessed September 27, 2022, at <https://doi.org/10.3133/ofr20041207>, at <https://water.usgs.gov/nrp/gwsoftware/SutraMS/OFR2004-1207.pdf>.
- Hughes, J.D., Langevin, C.D., and Banta, E.R., 2017, Documentation for the MODFLOW 6 framework: U.S. Geological Survey Techniques and Methods, book 6, chap. A57, 36 p., <https://doi.org/10.3133/tm6A57>.
- Kavetski, D., and Kuczera, G., 2007, Model smoothing strategies to remove microscale discontinuities and spurious secondary optima in objective functions in hydrological calibration: Water Resources Research, v. 43, no. 3, <https://doi.org/10.1029/2006WR005195>, <https://agupubs.onlinelibrary.wiley.com/doi/abs/10.1029/2006WR005195>.
- Kipp, K.L., 1987, HST3D: A Computer Code for Simulation of Heat and Solute Transport in Three-Dimensional Ground-Water Flow Systems: U.S. Geological Survey Water-Resources Investigation Report 86-4095, 517 p., accessed September 27, 2022, at <https://pubs.usgs.gov/wri/1986/4095/report.pdf>.
- Langevin, C.D., Thorne Jr, D.T., Dausman, A.M., Sukop, M.C., and Guo, W., 2008, SEAWAT Version 4—A computer program for simulation of multi-species solute and heat transport: U.S. Geological Survey Techniques and Methods, book 6, chap. A22, 39 p., accessed June 27, 2017, at <https://pubs.er.usgs.gov/publication/tm6A22>.
- Langevin, C.D., Hughes, J.D., Provost, A.M., Banta, E.R., Niswonger, R.G., and Panday, S., 2017, Documentation for the MODFLOW 6 Groundwater Flow (GWF) Model: U.S. Geological Survey Techniques and Methods, book 6, chap. A55, 197 p., <https://doi.org/10.3133/tm6A55>.
- Langevin, C.D., Provost, A.M., Panday, S., and Hughes, J.D., 2022, Documentation for the MODFLOW 6 Groundwater Transport (GWT) Model: U.S. Geological Survey Techniques and Methods, book 6, chap. A61, 56 p., <https://doi.org/10.3133/tm6A61>.
- Maidment, D.R., 1993, Handbook of Hydrology: New York, USA, McGraw-Hill.
- Panday, S., Langevin, C.D., Niswonger, R.G., Ibaraki, M., and Hughes, J.D., 2013, MODFLOW-USG version 1—An unstructured grid version of MODFLOW for simulating groundwater flow and tightly coupled processes using a control volume finite-difference formulation: U.S. Geological Survey Techniques and Methods, book 6, chap. A45, 66 p., accessed June 27, 2017, at <https://pubs.usgs.gov/tm/06/a45/>.
- Provost, A.M., Langevin, C.D., and Hughes, J.D., 2017, Documentation for the “XT3D” Option in the Node Property Flow (NPF) Package of MODFLOW 6: U.S. Geological Survey Techniques and Methods, book 6, chap. A56, 46 p., <https://doi.org/10.3133/tm6A56>.

## **R-2 MODFLOW 6 – Supplemental Technical Information**

- Voss, C.I., 1984, SUTRA—A finite-element simulation model for saturated-unsaturated fluid-density-dependent ground-water flow with energy transport or chemically-reactive single-species solute transport: U.S. Geological Survey Water-Resources Investigations Report 84-4369, 409 p.
- Zheng, C., 2010, MT3DMS v5.3, Supplemental User's Guide: Technical Report Prepared for the U.S. Army Corps of Engineers, 51 p.
- Zheng, C., and Wang, P.P., 1999, MT3DMS—A modular three-dimensional multi-species transport model for simulation of advection, dispersion and chemical reactions of contaminants in groundwater systems; Documentation and user's guide: Contract report SERDP-99-1: Vicksburg, Miss., U.S. Army Engineer Research and Development Center, 169 p.

Publishing support provided by the U.S. Geological Survey  
MODFLOW 6 Development Team

For information concerning this publication, please contact:

Integrated Modeling and Prediction Division  
U.S. Geological Survey  
Mail Stop 411  
12201 Sunrise Valley Drive  
Reston, VA 20192  
<https://www.usgs.gov/mission-areas/water-resources>

